K L Hallam

THE ATOMIC HYDROGEN MASER

H. Mark Goldenberg

November 1960

LYMAN LABORATORY OF PHYSICS
HARVARD UNIVERSITY - CAMBRIDGE, MASSACHUSETTS

THE ATOMIC HYDROGEN MASER

H. Mark Goldenberg

November 1960

Lyman Laboratory of Physics

Harvard University, Cambridge, Mass.

Table of Contents.

Table of Contents (Cont)

ABSTRACT

The research to be described has been supported in part by the Office of Naval Research under Contract Nonr-1866(19) and by the National Science Foundation under NSF G-10021. This report is the second half of a doctoral thesis submitted to the Physics Department of Harvard University. The first half is being submitted for publication to the Physical Review, and describes measurements of the hyperfine frequency of cesium which is perturbed by collisions with coated walls. It was found that for saturated hydrocarbon coatings, resonances were observed after as many as 200 bounces. The conclusion of the experiment was that in the case of atomic hydrogen, a greatly increased number of bounces should be possible.

An atomic hydrogen maser apparatus has been constructed and maser oscillation at the hydrogen hyperfine frequency has been observed. Relaxation times of .3 seconds have been measured corresponding to approximately 10,000 wall collisions. The theory of the maser is described as well as those factors affecting the stability of the maser as an oscillator. The characteristics of the pulsed and CW maser are described. Generalized magnet calculations are presented in an Appendix.

CHAPTER V

INTRODUCTION

The first part of this paper has described an experiment in which the atomic beam separated oscillatory field technique was applied to the measurement of the hyperfine frequency of cesium which is perturbed by collisions with storage box walls. It was found that for wall coatings of straight saturated hydrocarbons, resonances could be observed after as many as 200 wall collisions. From the results of this experiment it was concluded that in the case of atomic hydrogen, the tolerable number of wall collisions might well exceed 100,000. With this number of collisions, storage times of on the order of seconds can be realized, enabling spectroscopic measurements of unprecedented precision.

Those wall coatings which gave the best results with cesium are also expected to work with hydrogen in a stored beam experiment, but the beam technique is made prohibitively difficult by the problem of detection of the atomic hydrogen. However, the anticipation of extremely long storage times suggests the possibility of directly observing maser oscillation at the hydrogen hyperfine frequency (GOR 55).

Maser action with free atoms has not been previously observed up to this experiment due to the weakness of their radiation matrix elements. For atoms, the characteristic magnetic dipole matrix element is about 100 times smaller than the corresponding electric dipole matrix element of molecules, such as used in the ammonia maser (GOR 55). Although

criteria for maser oscillation depend on the square of these matrix elements, this factor can be compensated for by a large increase in the average time of interaction between the atoms and fields of the cavity. For an atomic hydrogen maser oscillator, average interaction times approaching one second are required.

An atomic hydrogen maser device has been constructed which utilizes the stprage box principle to obtain the requisite interaction times. Oscillation at the hyperfine frequency has been observed, and mean interaction times of 0.3 seconds have been measured using storage bulbs coated with paraffins or Dri-Film (dimythldichlorosilane). These relaxation times suggest the hydrogen atoms are not significantly perturbed after as many as 10,000 collisions with coated walls. The width of the hyperfine line is about 1 cps, which corresponds to a Q exceeding 10^9. In hte case where the critical requirements for oscillation are not met, stimulated emission in the hydrogen can be observed using a pulse technique.

The following chapter gives a description of the apparatus and associated pulse and frequency stabilization circuitry. In Chapter VII, the theory of the atomic hydrogen maser is discussed as well as those factors which affect its stability as an oscillator. The theory for the pulsed stimulated emission is also described. The final chapter describes some preliminary results on the measurement of the hyperfine structure separation in hydrogen. Characteristics of the pulsed and CW maser are discussed. A collection of useful field quantities, and generalized magnet solid angle calculations are presented in the appendices.

CHAPTER VI

APPARATUS

A schematic diagram of the apparatus is seen in Figure 19. A beam of hydrogen atoms is produced in a Wood's discharge tube. Those atoms in the F=1 m_F=0 state are focussed by a six-pole electromagnet into the entrance aperture of a coated quartz bulb located in a microwave cavity. The cavity is tuned to the frequency of the hyperfine transition, approximately 1420 mc/sec. A microwave pulse at this frequency with an appropriate amplitude and duration places atoms in the bulb in a radiating state. The decay of energy from the cavity after such a 90° pulse measures the lifetime of atoms in the bulb. If this relaxation time is sufficiently long, the power radiated by the beam can overcome cavity losses and maintain a relatively high power level in the cavity. Under these conditions the maser oscillates spontaneously without external pulsing.

The following sections describe the apparatus and associated equipment.

Vacuum System

The vacuum envelope consists of a source chamber housing the Wood's discharge tube and a detector chamber consisting of the beam tube and storage box. The two chambers are connected by a 1/2" diameter tube, 12" long, which passes through the gap of the magnet. There is a circular stop 3/16" in diameter at the entrance to the

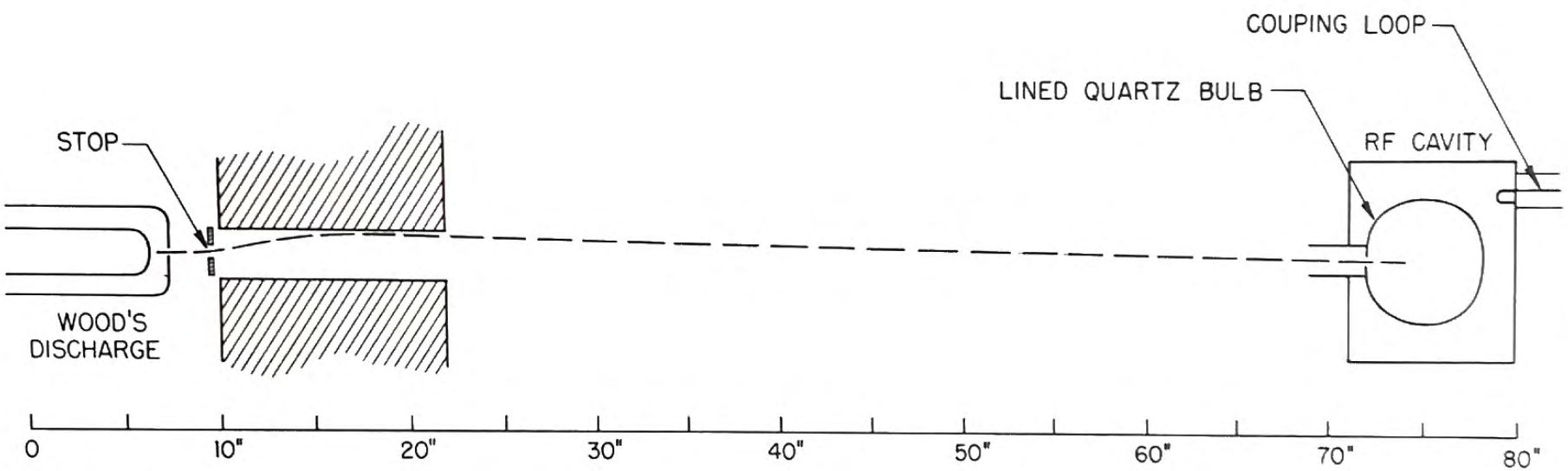

FIG. 19 SCHEMATIC DIAGRAM OF APPARATUS

magnet tube. The main part of the beam tube is 4" in diameter and 36" long and connects to the entrance aperture of the storage box. The source chamber is pumped by an Edwards 6M3 mercury diffusion pump through a liquid nitrogen trap. The baffle chamber is pumped by a similar Edwards pump through two traps, one of which is bakeable. Most demountable joints in the system are sealed with aluminum O-rings, which are discussed in Chapter III. The discharge tube flange and the microwave cavity flange are both sealed with neoprene or teflon O-rings and are the only non-bakeable sections of the apparatus. With the beam off, the pressure in the beam tube chamber is about 3×10^{-8} mm; with the beam on this rises to about 2×10^{-7} mm, with a source chamber pressure of 2×10^{-5} mm.

Source

Atomic hydrogen is produced by means of a high voltage DC discharge. Figure 20 is a diagram of the Wood's discharge tube. Water cooled aluminum electrodes are sealed through the ends of a pyrex U-tube. The tube, 11 mm heavy-walled Pyrex, is cooled over half its length within a circulating water jacket. A thin quartz disk with a .030" diameter hole is waxed to a ground seal at the U bend, forming the source aperture. The tube and jacket assembly is mounted on a bellows arrangement, and can be aligned by means of two micrometer screws. Molecular hydrogen is fed to the discharge tube through a calibrated leak valve. The discharge runs stably at a hydrogen pressure of several tenths of a millimeter Hg. The dissociation efficiency of the source seems to be improved by coating

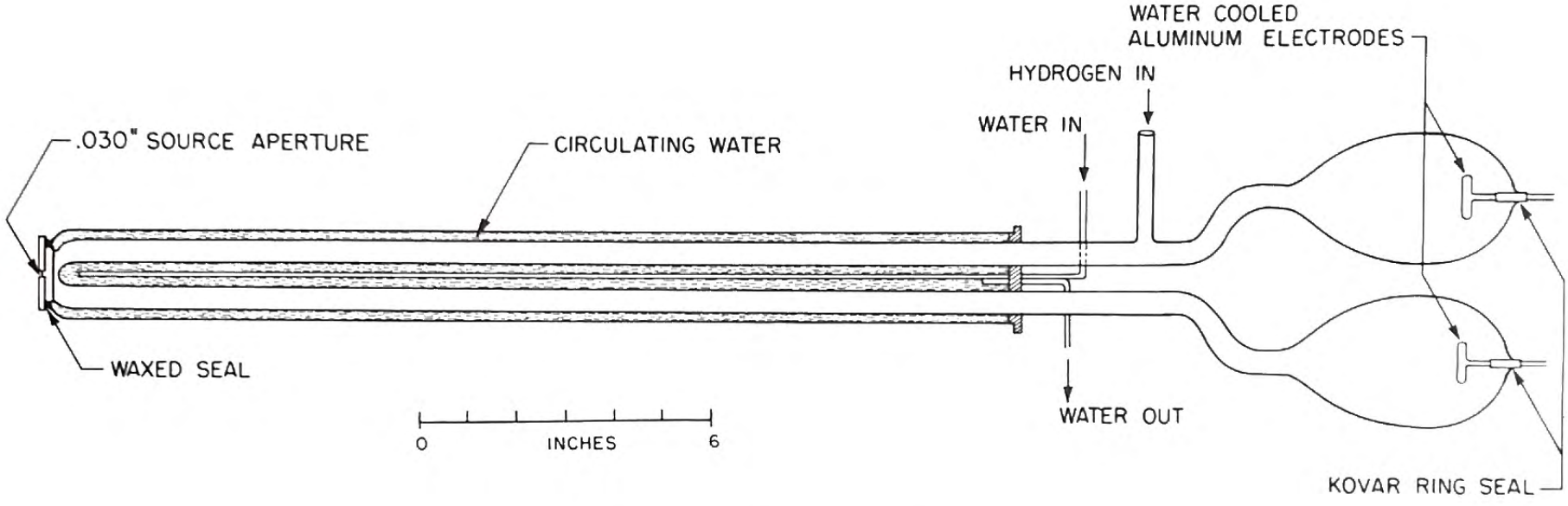

FIG. 20 WOOD'S DISCHARGE TUBE

with Dri-Film, also a successful coating for storage box walls. The discharge is run at about 4 kv and draws a direct current of approximately 150 ma.

State Selecting Magnet

The state selector is the B magnet of the Cesium experiment, and is described in Chapter III. The calculated effective solid angle of this magnet for atoms in the F=1 m_F=0 state to be focussed into the .080" entrance aperture of the storage box is 6×10^{-5} ster. For a discharge tube pressure of 0.1 mm Hg and source aperture of .030", this corresponds to a flux of atoms in the correct state to the quartz bulb of 3×10^{12} sec^{-1}. In practice, the source is run at several tenths of a mm pressure. Calculations for the effective solid angle of the magnet are given in Appendix A.

Storage Boxes

In this experiment, the storage box also serves as part of the vacuum envelope. It must be capable of withstanding atmospheric pressure and must have a low microwave loss factor to not degrade the cavity Q. Most glasses do not meet the latter requirement, and fused quartz was chosen (Syn 60). Bulbs were used ranging in diameter from 3 to 6 inches, and with apertures of from 7 to 9 mm. All bulbs have wall thicknesses of 1 mm and were supported by two collinear tubes on opposite diameters of the sphere. One of the support tubes was sealed off next to the sphere, while a small hole in a disk in the other tube formed the entrance aperture. The

entrance tube was sealed by a neoprene O-ring through a small hole in the cavity flange.

Two wall coatings have been used with success; paraflint and Dri-Film (Gen 60). Dri-Film coated bulbs were used in most of the work, however, as it could be more easily and reliably applied on the quartz. The bulbs were first prepared by several boilings in dichromate solution, followed by many distilled water rinses. The Dri-Film was injected in the bulbs through a hypodermic needle. An excess was injected to ensure complete contact with the interior surface. After draining, the bulbs were roughed by a small mechanical pump before being placed in the apparatus.

Paraflint has also been used successfully in the cesium experiment, and is fully discussed in Chapter IV. In this case, the paraflint was coated on the quartz in great excess, to ensure complete coverage. The excess was drained out when molten. The paraflint coated bulbs were less convenient than those using Dri-Film as they invariably required baking at some temperature above the paraflint melting point.

MicrowaveCavity and Helmholz Coils.

The hyperfine frequency of hydrogen lies at approximately 1420 mc/sec, a wavelength of about 21 cm. A cylindrical cavity resonant at this frequency in the TE_{011} mode was chosen because it has a magnetic field along the axis whose phase is constant over a cylindrical region of .63 the cavity radius and of the full cavity length. This mode has the additional advantage of having current nodes

at the end joints, which allows high Q without careful machining. The field equations appropriate to this mode are

$$H_z = H_o J_o(kr) \sin\left(\frac{\pi z}{L}\right)$$

$$H_r = \frac{\pi}{kL} H_o J_o'(kr) \cos\frac{\pi z}{L}$$

$$H_\theta = 0$$

where L is the length and 2a the diameter of the cavity. Also

$$k^2 + \frac{\pi^2}{L^2} = (2\pi/\lambda)^2$$

$$J_o'(ka) = 0$$

Several field averages of importance in this experiment are compiled in Appendix B.

The cavity has a diameter of 11", a length of 14". It is made of fused quartz and has its inside surface silver plated. Its normal resonant length is about 11", but this reduces to about 9" when the cavity is loaded by a typical 6" diameter quartz bulb. The TE_{011} mode is degenerate with the TM_{111} mode, but the bulb splits the degeneracy completely. The cavity is tuned by a movable end plate mounted on a partially temperature compensated support.

A single coupling loop can be rotated to provide a variable loading of the cavity. The unloaded Q exceeds 80,000, and this value is reduced by no more than a few percent by the quartz bulb.

Since the rf field points along the z or beam axis, the magnetic field of the earth must be compensated. Three sets of

Helmholz coils were constructed for this purpose. The vertical component of the earth's field is cancelled by a set of 48" diameter and 36" separation. The horizontal field cancelling coils are of 27" diameter and 20" separation, while the Z field coils are of 35" diameter and 25" separation. The calculated homogeneity over a 6" sphere at their common center is about 6 milligauss.

Microwave Receiver and Frequency Stabilization.

The power to be expected from the maser is approximately 10^{-12} to 10^{-13} watts. As the power spectrum is only about 1 cps wide, the inherent signal to noise ratio is extremely high if the narrow band of the line can be utilized. The stimulated emission from the cavity was observed by two techniques; pulse and CW. The latter scheme was only applicable when the maser was spontaneously oscillating, although the pulse technique could be used when the conditions for oscillation were not met.

Figure 21 is a schematic diagram of the detector arrangement used with the pulse technique. Microwave tuning elements have not been indicated. The Gertsch FM-4A provides local oscillator power for the klystron lock-in circuit, while the beat reference signal is supplied by the Gertsch AM-1. In addition the same two oscillators provide local oscillator power and reference signal to the receiver which allows coherent detection.

The klystron pulse is attenuated by a variable waveguide-beyond-cutoff and is loop-coupled into the end plate of the cavity through the side arm of a 10 db directional coupler. Signal power from

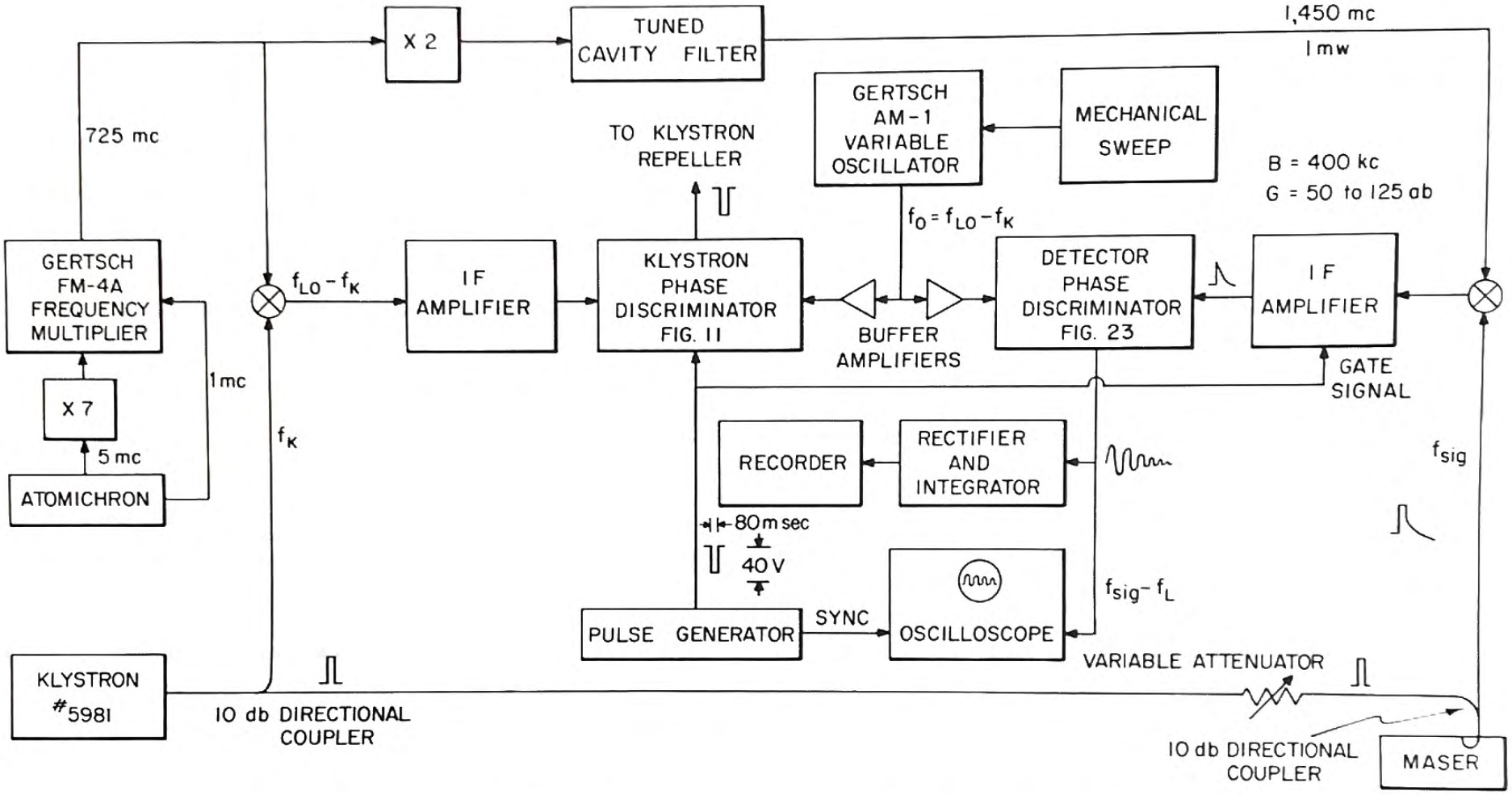

FIG. 21 COHERENT RECEIVER FOR PULSE PHASE-LOCKED TECHNIQUE

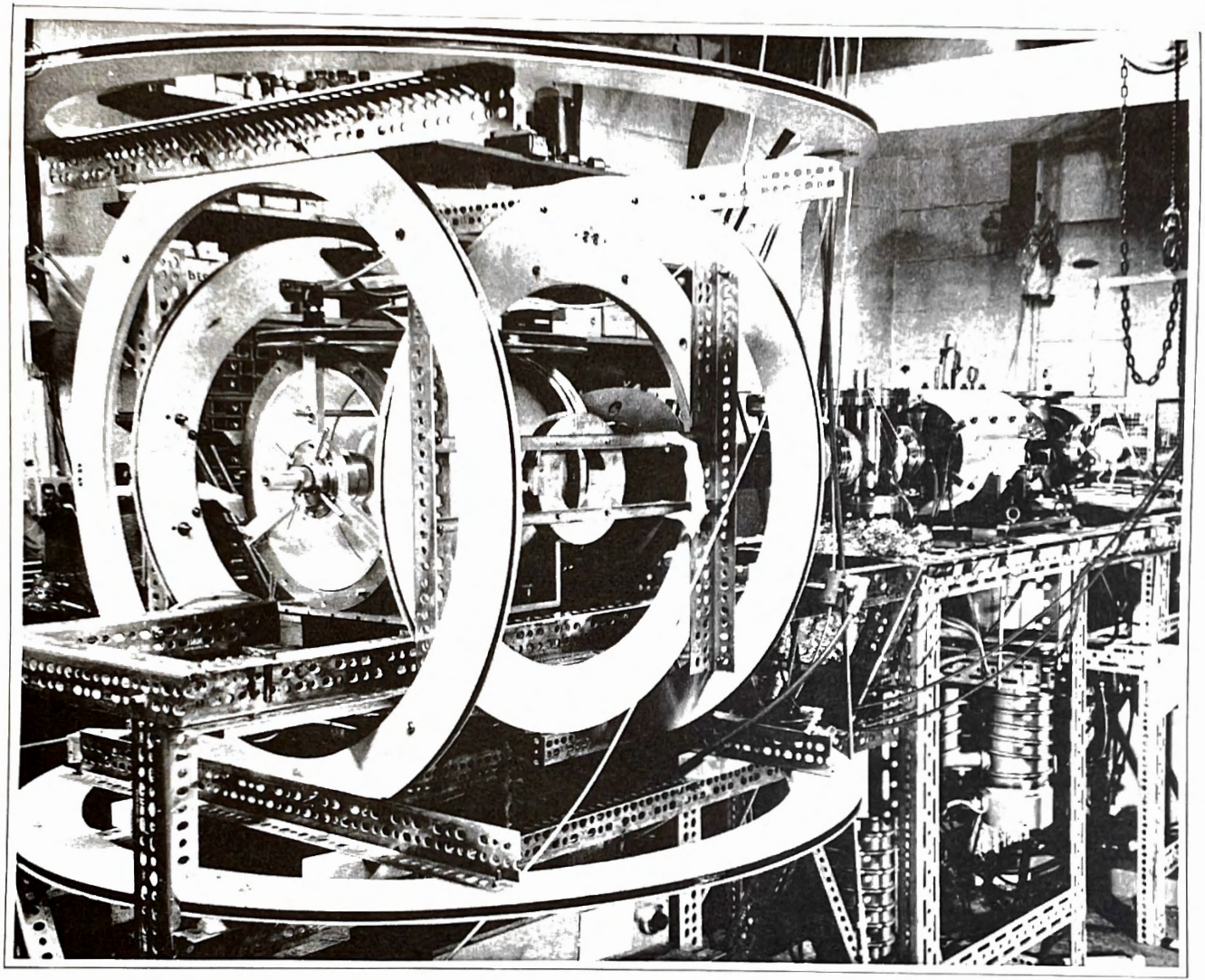

FIG. 22 OVERALL VIEW OF THE APPARATUS

the cavity is coupled out by the same loop through the straight arm of the directional coupler to a single ended balanced mixer. (SAG 60). The signal passes through a preamplifier (IFI No. 205A), a 400 kc tuned amplifier and a broadband amplifier (IFI No. M235) of variable gain. The overall gain can be varied between 40 and 120 db. The IF amplifier is followed by the dual diode phase discriminator shown in Figure 23. This circuit mixes the detected signal with the AM-1 and presents an output at the difference frequency of the klystron and the hydrogen signal whose amplitude decays with the characteristic relaxation time of the hydrogen. A typical oscilloscope trace is seen in Figure 26. The decay rate of the envelope provides a direct measure of the relaxation time for atoms within the bulb. If the klystron is swept, the train of decaying signals can be rectified and integrated for recorder display of line shape.

The hydrogen hyperfine frequency measurements were most conveniently made with the maser oscillating. Figure 24 is a block diagram of the detector used for these measurements. The circuit for the 29.6 mc/sec synthesizer is given in Figure 25. It is seen that all frequencies are synthesized directly from standard outputs from an Atomichron with the exception of the 100 kc/sec time base for the counter. The stability of the counter 100 kc is not a source of error, and a small fixed correction is made for absolute calibration of the signal. The stability of the counted frequency was then limited only by the fluctuations in the Atomichron and noise generated in the synthesizing circuitry.

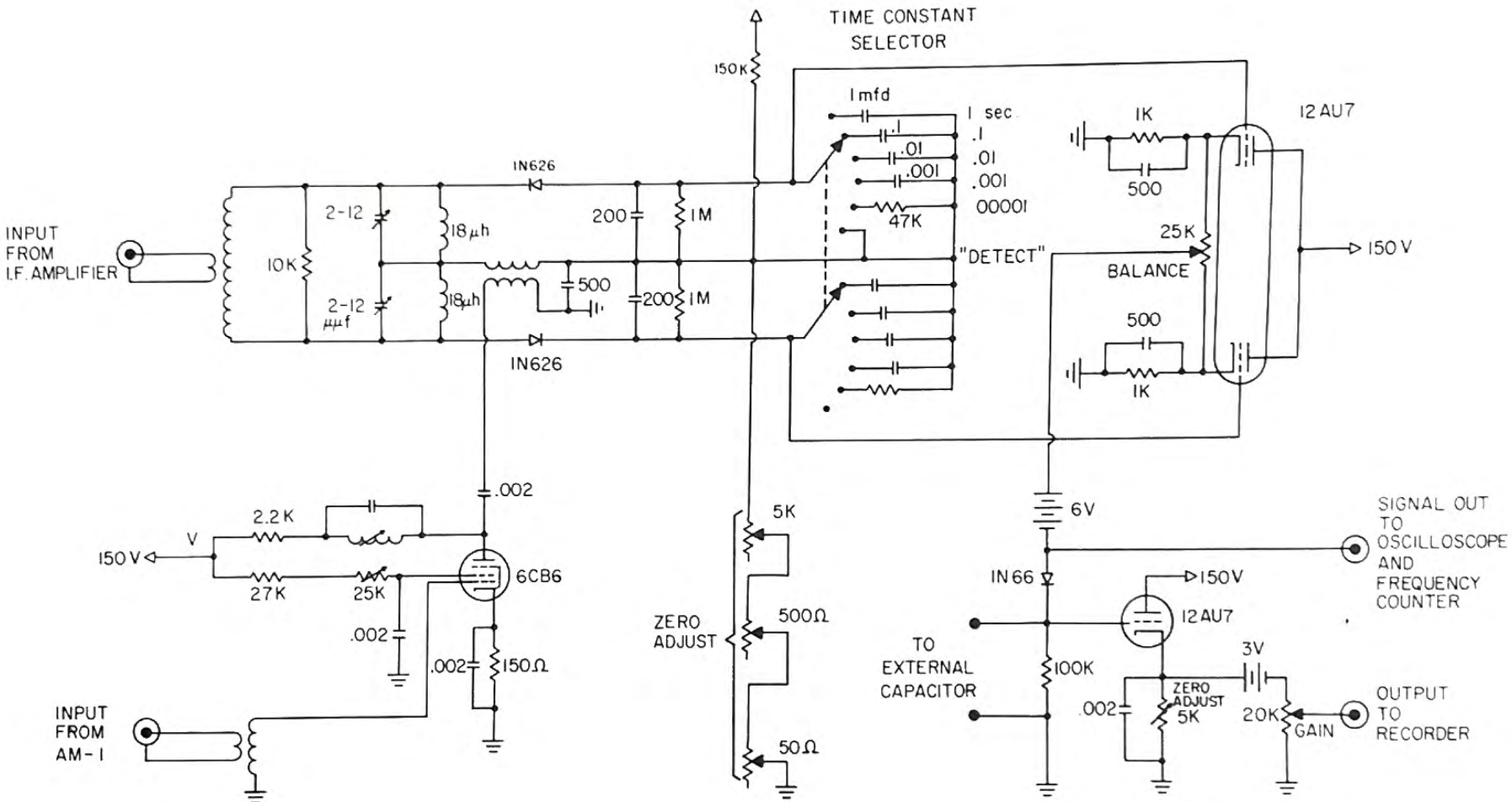

FIG. 23 DETECTOR PHASE DISCRIMINATOR

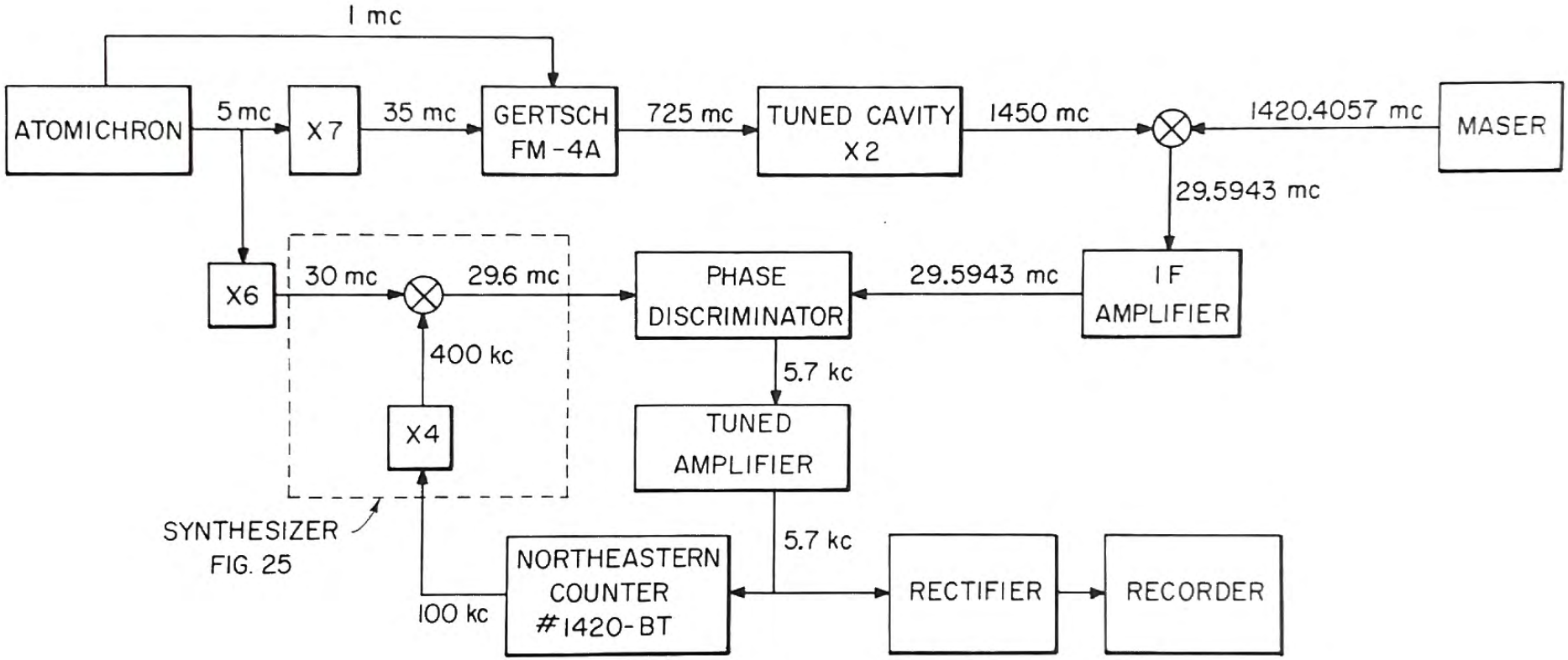

FIG. 24 RECEIVER FOR C W MASER

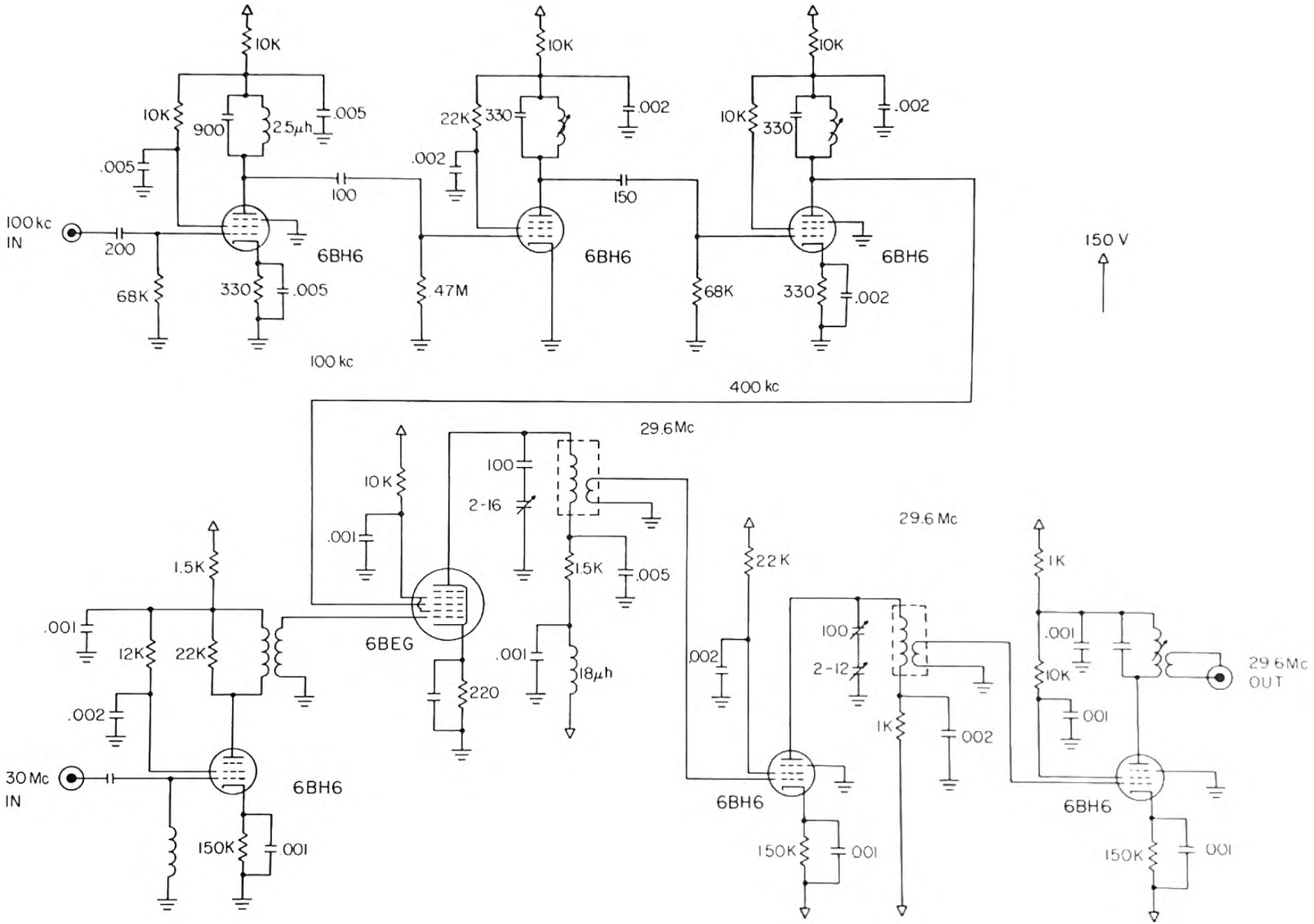

FIG. 25 29.6 Mc SYNTHESIZER

Stability of the Frequency Standard

The primary frequency standard used in this experiment was the Atomichron which is operated and monitored by J. R. Pierce in the Cruft Laboratory. The long term stability of this device is about 1 part in 10^{10}, and over any period of a few hours, its average frequency could be checked against several other standards. However, over consecutive ten second counting intervals, fluctuations in the converted signal from the maser of up to 1 cps, about one part in 10^{9}, were observed. It is believed that the fluctuations were due to instability in the servo system of the Atomichron. This hypothesis was strengthened by substituting a second Atomichron as the standard. This Atomichron was located in our laboratory, and had a lower gain in the servo loop than the Pierce Atomichron. With this Atomichron, the spread in consecutive ten second counts were typically 0.3 cps, where 0.2 cps represents the counting uncertainty inherent to the counter.

CHAPTER VII

THEORY

The theory of the ammonia maser has been well described in the literature (GOR 55), (SHI 56). With several modifications it can be carried over to a description of the atomic hydrogen maser. We first derive the dynamical equations of the system in an integral form particularly useful for describing transient phenomena.

Dynamical Equations

Proceeding from the Schroedinger equation

$$ih\frac{d\psi}{dt} = [H_o + V(t)]\psi \tag{6.1}$$

with $$V(t) = -\mu \cdot H(t) \cos wt$$

we look for the transition probability between the two states of interest, ψ_1 and ψ_2, of energy E_1 and E_2, as induced by the perturbation $V(t)$ which is assumed of constant frequency and variable amplitude. The wave function at any time can be written

$$\psi(t) = a_1(t)\psi_1 e^{-\frac{iE_1}{h}t} + a_2(t)\psi_2 e^{-\frac{iE_2}{h}t} \tag{6.2}$$

which when substituted above leads to the equations

$$\dot{a}_1(t) = \frac{V_{12}(t)}{ih} e^{-iw_o t} a_2(t)$$

$$\dot{a}_2(t) = \left(\frac{V_{12}(t)}{ih} e^{-iw_o t}\right)^* a_1(t) \tag{6.3}$$

$$w_o = [E_2 - E_1]/h$$

where $V_{12}(t)$ is the matrix element of $V(t)$ between the states 1 and 2. The perturbation can be written to good approximation as

$$V(t) = -\frac{1}{2}\mu H(t)e^{iwt}$$

or

$$V_{12}(t) = -\frac{hb}{2}e^{iwt}$$

where

$$b = b(t) = \frac{\mu_o H(t)}{h} . \tag{6.4}$$

Substituting into (6.2), one obtains

$$\ddot{a}_1 - \dot{a}_1\left[\frac{\dot{b}}{b} + i(w - w_o)\right] + (b/2)^2 a_1 = 0 \tag{6.5}$$

and assuming resonance, $w = w_o$, the solutions

$$a_1(t) = -i \sin\left[\frac{1}{2}\int_0^t b(t)\,dt\right]$$

$$a_2(t) = + \cos\left[\frac{1}{2}\int_0^t b(u)du\right] \tag{6.6}$$

are seen to satisfy the differential equations (6.2) and the initial conditions $a_1(0) = 0$, $a_2(0) = 1$. The quantity of particular interest is the excess population in the lower state, $D(t) = N_1(t) - N_2(t)$, (BLO 56)

$$D(t) = N\left[|a_1(t)|^2 - |a_2(t)|^2\right]$$

or from (6.6)

$$D(t) = D(0)\cos\int_0^t b(u)du \tag{6.7}$$

The power radiated by the beam is simply given by

$$P_B = h\omega \frac{\dot{D}(t)}{2} \quad , \tag{6.8}$$

As discussed following (6.12), only that part of $\dot{D}(t)$ corresponding to radiative transitions is to be used in the above expression. The beam radiates with a microwave cavity, and therefore

$$P_B = \frac{\omega W}{Q} = \frac{\omega}{Q}\left[\frac{1}{4\pi}\int H^2\, dV\right] = \frac{\omega V_{eff}}{8\pi Q} H^2 \tag{6.9}$$

where the additional factor of 1/2 being due to the time average of H^2. Substituting (6.4), we have

$$h\omega \frac{\dot{D}(t)}{2} = \frac{\omega V_{eff} h^2}{8\pi Q \mu_o^2} b^2(t) = \alpha \dot{D}(t) \frac{\omega V_{eff} h^2}{8\pi Q \mu_o^2} \tag{6.10}$$

and generally $b^2 = \alpha \dot{D}(t)$, $\qquad \alpha = 4\pi \frac{\mu_o^2 Q}{h V_{eff}}$. $\tag{6.11}$

The equations of motion of the system follow easily from these results. We assume a uniform flux into the cavity of I upper state atoms per second. If $1/\gamma$ denotes the characteristic relaxation time, then by (2.1)

$$I\, dt'\, e^{-\gamma(t - t')}$$

is that number of atoms which entered between time t' and $t' + dt'$ which have not relaxed by time t. It is assumed that the relaxation mechanism acts on each state equally, and carries atoms to states other than 1 and 2. Thus applying (6.7)

$$dD(t) = \frac{\partial D(t)}{\partial t'} dt' = \left[(-I dt') \cos \int_{t'}^{t} b(u)\, du \right] e^{-\gamma(t - t')} \tag{6.12}$$

is the contribution to the excess population in the lower state at time t due to atoms which entered between t' and t' + dt'. It should be pointed out the time time derivative of (6.12) consists of two terms

$$\frac{d}{dt}[\, dD(t)] = -\gamma dD(t) + I dt' \, b(t) \sin \int_0^t b(u)du \quad .$$

As the first term is just the diminution of the excess lower population due to the relaxation mechanism, it does not correspond to radiation of power by the beam. In calculating power with (6.8) and (6.10), terms of this form are therefore to be neglected. Continuing, if the beam is turned on at time t_o, we have by integration of (6.12)

$$D(t) = \int_{t_o}^{t} dt' \, (-I)[\cos \int_{t'}^{t} b(u)du] e^{-\gamma(t - t')} \qquad (6.13)$$

as the net excess population in the lower state at time t due to all atoms which have entered since t_o, the turn-on time. This result together with (6.10) represents the solution to maser transient problems. The general problem does not have a solution in closed form, although the equations are useful for several interesting limiting cases.

Threshold Conditions

We consider first the steady state operation of the maser corresponding to $t_o = -\infty$, in (6.13). In the steady state we have b(t) a constant = b, and

$$D(t) = \int -I \, dt' \cos b(t - t') e^{-\gamma(t - t')} \quad ,$$

$$\dot{D}(t) = \int_{-\infty}^{t} -I\, dt'\, b \sin b(t - t') e^{-\gamma(t - t')}.$$

The time derivative has been taken as discussed in the previous section.

Integrating

$$\dot{D}(t) = \frac{b^2}{\gamma^2 + b^2} I.$$

Substituting, (6.8)

$$P_B = \frac{Ihw}{2} \frac{(b/\gamma)^2}{1 + (b/\gamma)^2} = \frac{Ihw}{2} \frac{\theta^2}{1 + \theta^2}. \qquad (6.14)$$

where

$$\theta^2 = (b/\gamma)^2 \qquad (6.15)$$

but, (6.10)

$$P_B = \frac{hw}{2} \dot{D}(t) = \frac{hw}{2} \frac{b^2}{\alpha} = \frac{hw\gamma^2}{2\alpha} \theta^2. \qquad (6.16)$$

Equating (6.16) and (6.14),

$$I = (1 + \theta^2) \frac{\gamma^2}{\alpha} \qquad (6.17)$$

which relates the steady state flux to the saturation factor θ, and the relaxation time, $1/\gamma$. The critical flux for oscillation is given by $\theta \rightarrow 0$, or

$$\frac{I}{I_{crit}} = (1 + \theta^2) \qquad (6.18)$$

where the critical flux is simply, (6.11)

$$I_{crit} = \frac{\gamma^2}{\alpha} = \frac{\gamma^2 V_{eff}}{\mu_o^2 Q} h \quad . \qquad (6.19)$$

Inserting numerical values, $Q = 5 \times 10^4$, $V_{eff} = 10^4$ cm^3, $\gamma = 3$ sec^{-1}, one obtains $I_{crit} = 2 \times 10^{13}$ sec^{-1}.

Taking eqns 18,17, and 14, there follows

$$\theta^2 = \left[\frac{I - I_{crit}}{I_{crit}} \right]$$

$$P_B = \frac{hw}{2} \left[I - I_{crit} \right] . \qquad (6.20)$$

The radiated power from the maser is typically 5×10^{-12} watts, corresponding to a flux of atoms in the (1,0) state into the cavity of approximately 3×10^{13} sec^{-1}.

Maser Turn-Off Time

Assume the maser is oscillating in a steady state condition and that at time t = 0, the beam is interrupted. Then, by (6.13), we have for time $t > 0$

$$D(t) = \int_{-\infty}^{0} -I dt' \, e^{-\gamma(t - t')} \cos \int_{t'}^{t} b(u) du$$

The upper limit of the t' integral is 0 since atoms enter the cavity for $t' < 0$ only. Taking the time derivative of this expression in the sense discussed following (6.12), we have

$$\dot{D}(t) = \int_{-\infty}^{0} I dt' \, e^{-\gamma(t - t')} \, b(t) \sin \int_{t'}^{t} b(u) du .$$

Then,

$$\dot{D}(t) = -I e^{-\gamma t} b(t) \cos \int_{0}^{t} b(u) du \int_{-\infty}^{0} dt' e^{\gamma t'} \sin b_o t'$$

$$+ I e^{-\gamma t} b(t) \sin \int_{0}^{t} b(u) du \int_{-\infty}^{0} dt' e^{\gamma t'} \cos b_o t'$$

where we have used $b(t) = b_o$ = constant, for $t < 0$. Integrating over t' and applying (6.11), we obtain the expression for b(t), $t > 0$.

$$b(t) = \frac{b_o\gamma}{\gamma^2+b_o^2}\, e^{-\gamma t}\cos\int_0^t b(u)du \;+\; \frac{I\gamma^2}{\gamma^2+b_o^2}\, e^{-\gamma t}\sin\int_0^t b(u)du.$$

Substituting as follows $\lambda(t) = \int_0^t b(u)du\,, \qquad \dot{\lambda}(t) = b(t)$

we find

$$\dot{\lambda}(t) = [\; b_o\cos\lambda(t) + \gamma\sin\lambda(t)\;]\, e^{-\gamma t} \tag{6.21}$$

where we have made use of (6.15) and (6.18). Furthermore, by defining the angle β such that $\sin\beta = b_o/\sqrt{b_o^2+\gamma^2}$, $\cos\beta = \gamma/\sqrt{b_o^2+\gamma^2}$ we obtain

$$\dot{\lambda}(t) = \sin[\;\beta + \lambda(t)\;]\sqrt{b_o^2+\gamma^2}\;\; e^{-\gamma t}.$$

The equation is separable

$$\frac{d\lambda}{\sin(\lambda+\beta)} = dt\; e^{-\gamma t}\sqrt{b_o^2+\gamma^2}$$

and integrating,

$$\log\tan(\lambda+\beta)/2 = \log\tan\beta/2 \;\; +\sqrt{b_o^2+\gamma^2}\;(1-e^{-\gamma t})$$

which satisfies the initial condition $\lambda(0) = 0$. Rewriting as

$$\log\tan[\;\tfrac{\pi}{4}+\tfrac{\lambda}{2}+\tfrac{\beta}{2}-\tfrac{\pi}{4}\;] = u(t)$$

we identify gd $u = \lambda + \beta + \pi/2$, where we have the relation

$$\frac{d}{du}\,\mathrm{gd}\;u = \mathrm{sech}\;u$$

or

$$\dot{\lambda}(t) = b(t) = \sqrt{b_o^2+\gamma^2}\; e^{-\gamma t}\;\mathrm{sech}[u(t)]$$

which is seen to satisfy the initial condition $b(0) = b_o$, making use of the identity sech log $\tan\beta/2 = \sin\beta$. Furthermore, sinh log $\tan\beta/2 = \cot\beta$, and cosh log $\tan\beta/2 = \csc\beta$, with the simplification

$$b(t) = \frac{b_o e^{-\gamma t}}{\cosh\left[\frac{\sqrt{\gamma^2+b_o^2}}{\gamma}(1-e^{-\gamma t})\right] + \cos\beta \sinh\left[\frac{\sqrt{\gamma^2+b_o^2}}{\gamma}(1-e^{-\gamma t})\right]}$$

Substituting into (6.16), we obtain for the power radiated by the beam after turn-off

$$P_B = \frac{hwb^2}{2\gamma} = \frac{P_o e^{-2\gamma t}}{\left[\cosh\left[\frac{\sqrt{\gamma^2+b_o^2}}{\gamma}(1-e^{-\gamma t})\right] + \cos\beta \sinh\left[\frac{\sqrt{\gamma^2+b_o^2}}{\gamma}(1-e^{-\gamma t})\right]\right]^2} \quad . \quad (6.22)$$

Pulsed Stimulated Emission

If the threshold requirements for oscillation are not met, a pulse technique can be used to excite the hydrogen to states from which it emits coherent radiation. The pulse places atoms into a superposition of the (1,0) and (0,0) states , in which the magnetic dipole moment has oscillatory components at right angles to the static field. The atoms can be described by a net magnetization vector which can be treated classically in determining their radiation rate (DIC 54). The subsequent decay of radiation after the perturbing pulse gives a measure of the lifetime or relaxation time within the bulb.

The method introduced in the first part of this chapter may be applied to the calculation of the response of the maser to pulsed rf. The contribution to the excess lower population after the pulse can be found in this case by summing three terms\ the first is that contribution from atoms entering the bulb before the pulse, the second term is that due to atoms entering during the pulse, and

lastly the contribution to D(t) of those atoms entering after the pulse.

Whereas these equations can readily be obtained by inspection, the general solution does not exist in elementary form. A simple case of interest that can be solved exactly is that in which the contributions to D(t) are negligible for atoms entering during and after the pulse. In this case, from (6.13), the excess lower population is just

$$D(t) = -\frac{I_o}{\gamma} e^{-\gamma t} \cos\left[\theta + \int_0^t b(u)du \right]$$

where

$$\theta = b_{rf}\tau$$

as determined by the pulse is normally chosen as $\pi/2$. Differentiating as discussed previously, one obtains

$$D(t) = \frac{I_o}{\gamma} e^{-\gamma t} b(t) \cos \int_0^t b(u)du$$

and from (6.11),

$$b(t) = \frac{\alpha I_o}{\gamma} e^{-\gamma t} \cos \int_0^t b(u)du \ . \qquad (6.23)$$

This equation has the solution

$$b(t) = \frac{\alpha I_o}{\gamma} e^{-\gamma t} \operatorname{sech}\left[\exp\left(-\frac{\alpha I_o}{\gamma^2} e^{-\gamma t}\right)\right] ,$$

which is exact, although an interesting solution can be obtained from the small angle approximation of (6.23), in which case the cosine term is unity. Therefore, one obtains directly

$$b(t) = \frac{\alpha I_o}{\gamma} e^{-\gamma t}.$$

Substituting this solution into (6.10) and (6.11), one obtains for the power radiated by the beam after the pulse as

$$P_B = \frac{hwb^2}{2\alpha} = \frac{w\mu_o^2 I_o^2 Q}{\gamma^2 V_{eff}} e^{-2\gamma t}$$

$$P_B = P_{init} e^{-2\gamma t}$$

Inserting the numerical values $I_o = 3 \times 10^{12}$ sec^{-1}, $Q = 5 \times 10^4$, $V_{eff} = 10^4$ cm^3, and $\gamma = 3$ sec^{-1}, we find the initial rate of stimulated radiation at $P_{init} = 3 \times 10^{-4}$ watt. The small angle approximation is valid here since the critical flux for these conditions is 2×10^{13} sec^{-1}. If the beam flux is sufficiently low that the approximation holds, then the relaxation time can be measured as twice the characteristic decay time of this radiated power.

Line Shape

The derivation of the dynamical equations (6.11) and (6.13) followed from the solution of Schroedinger's equation for a perturbation at the resonance frequency with variable amplitude. Alternately, V(t) can be assumed to be of constant amplitude and variable frequency. Such an approach leads to information on line widths and power broadening (SHI 56). The discussion of equations 1-3 is carried over directly for this case. In analogy to (6.4), we have

$$V(t) = -\frac{\mu \cdot He^{iwt}}{2}$$

$$V_{12}(t) = -\frac{1}{2} hbe^{iwt}$$

where b is now a constant. The well known solution from perturbation theory follows

$$a_1(t) = -e^{i(w - w_o)t/2}\,\frac{b}{a}\sin[\,a(t - t_o)/2] \qquad (6.24)$$

$$a_2(t) = e^{-i(w - w_o)t/2}\left[-\frac{\lambda}{a}\sin a(t - t_o)/2 + i\cos\frac{1}{2}a(t - t_o)\right]$$

where $a = [\,(w - w_o)^2 + b^2\,]^{\frac{1}{2}}$

and $b = \mu_o H/h$.

The quantity $|a_1(t)|^2$ is the probability of finding an atom in the lower state at time t. The power radiated by the stored beam is then given by

$$P_B = hw\int_{-\infty}^{t} I dt'\, e^{-\gamma(t - t')}\,\frac{d}{dx}[\,|a_1(x)|^2]\,\Big|_{x=t-t'}$$

or

$$P_B = hw\int_{-\infty}^{t} I\,dt'\, e^{-\gamma(t - t')}\,\frac{b^2}{2a}\sin a(t - t')$$

$$P_B = hwIb^2\,\frac{1}{2(\gamma^2+a^2)} = \frac{Ihw}{2}\,\frac{\theta^2}{1+\delta^2+\theta^2} \qquad (6.25)$$

where

$$\delta^2 = [w - w_o]^2/\gamma^2$$

and θ^2 has been defined in (6.15). The line shape has a Lorentzian form, characteristic of an exponential time distribution. At resonance the distribution (6.25) reduces to (6.14) previously derived, so that this calculation is consistent with eqns 17-20. The line width at half power points can be found from the above expression

$$(w - w_o)/\gamma = \sqrt{1 + (b/\gamma)^2}$$

or $$2\Delta\nu_L = \frac{\gamma}{\pi}\sqrt{1 + \theta^2}$$

where it is seen that power broadening is appreciable for $\theta > 1$. Inserting numerical values $\theta^2 = 1$, and $\gamma = 3\ \text{sec}^{-1}$, as in previous examples, one obtains $2\Delta\nu_L = \sqrt{2}$ cps.

Maser Power Spectrum

The resonance line-width calculated above represents the response of the system to an external perturbation. When oscillating, the transitions are self-stimulated, and the spectral line-width of the oscillation, $\Delta\nu_m$, is considerably smaller. In the absence of external perturbations, the maser has a stability limited only by random noise in the cavity. An estimate of the power spectrum is obtained by the following argument. We approximate the center of the Lorentzian curve (6.25), by a parabola.

$$P_B(\nu) = P_o\left[\,1 - 2\left(\frac{\nu - \nu_o}{\Delta\nu_L}\right)^2\,\right].$$

If $\Delta\nu_m$ denotes the oscillating bandwidth, the beam is influenced by noise power in the bandwidth, of $kT\Delta\nu_m$. The center frequency of oscillation is uncertain to such extent that

$$P_B(\nu=\nu_o) - P_B\left(\nu=\nu_o \pm \frac{\Delta\nu_m}{2}\right) = kT\Delta\nu_m$$

or $$\Delta\nu_m = \frac{2kT}{P_o}(\Delta\nu_L)^2 .$$

A rigorous calculation has the result (GOR 55)

$$\Delta\nu_m = \frac{8\pi kT}{P_o}(\Delta\nu_L)^2$$

Inserting the numerical values previously obtained, $\Delta\nu_L = \sqrt{2}$ cps, $P_B = 10^{-12}$ watt, one finds $\frac{\Delta\nu_m}{\nu_m} = 10^{-17}$. This represents the

inherent width of the power spectrum at any time. The stability of the maser over a period long compared with $1/\gamma$ seconds will be discussed later in this chapter. However, the inherent stability may not be realized due to a number of systematic effects which shift the frequency. The remainder of this chapter is given to a discussion of the magnitudes of these various effects.

Frequency Deviations in the Maser

Shimoda, Wang and Townes (SHI 56) have analyzed in detail the frequency shifts in the ammonia maser due to a variety of perturbing influences. Some of these effects are also important in the hydrogen maser. With some modification, their results can be applied to these cases.

Wall Collision Effects

As discussed at length in Chapter II, the interaction between an atom and a surface can best be described in terms of a number, δ, the mean phase shift per collision. The shift in the resonance frequency of the line is related to the mean phase shift per collision δ, as

$$\Delta f = \delta/2\pi t_o$$

where Δf is the frequency shift and t_o is the mean wall collision time. A lower limit on δ can be inferred from the optical pumping results on pressure shifts in buffer gasses for atomic hydrogen (AND 60). We assume that the interaction between atomic hydrogen and the surface can never be less than that characterizing atomic hydrogen-molecular hydrogen gas collisions. The pressure shift for atomic hydrogen in a molecular hydrogen buffer gas is -0.24 cps/mm Hg. If this is equated in turn to $\delta/2\pi t_o$, where t_o is here the mean

collision time in the gas, one obtains $\delta = 6 \times 10^{-9}$ radians per collision. In the present work, the typical mean wall collision time for atomic hydrogen is about 3×10^{-5} sec. This places a lower limit on the frequency shift in these experiments at about 2×10^{-4} cps, or a shift of about one part in 10^{13}. We expect to observe larger shifts than parts in 10^{12}, however, and these figures are not particularly meaningful. The question of the constancy and reproducibility of the phase shift on the surface is one that must be answered experimentally.

Cavity Pulling

In the oscillating maser, the atomic hydrogen within the storage box has an induced oscillating magnetization which can be calculated assuming the given cavity field. The field generated by the magnetization can then be made consistent with the assumed field. In the case of no noise, they are simply equated. The following treatment parallels that of Shimoda et al (SHI 56).

The magnetic moment of an atom is

$$\mu = \int \Psi^* \mu_{op} \Psi \, d\tau = a_2^* a_1 \mu_{21} e^{i w_o t} + a_1^* a_2 \mu_{12} e^{-i w_o t}$$

where the amplitudes a_1 and a_2 satisfying the appropriate boundary conditions are given by (6.24). Substituting, we obtain

$$\mu(t) = \mu_o e^{iwt} \frac{x}{a}\left[\frac{i}{2} \sin at + \frac{\lambda}{a} \sin^2 \frac{1}{2} at \right] + c.c.$$

or

$$\mu(t) = \mu' e^{iwt} + \mu'^* e^{-iwt} .$$

If the flux into the storage box is I_o atoms per second, the net

magnetization is given by

$$M = \frac{1}{V_{eff}} \int_0^\infty I_o e^{-\gamma t} \mu(t) dt$$

where V_{eff} if the volume of the storage bulb, and $1/\gamma$ is the relaxation time. The magnetization can be considered a small perturbation to the normal mode of the cavity, and the cavity frequency can be calculated from the result of Slater (SLA 46),

$$\frac{1}{Q_m} - 2i \frac{w-w_c}{w_c} = \frac{1}{Q_c} - 4\pi i \frac{\int M^\dagger \cdot H^{\dagger *} dV}{\int H^\dagger \cdot H^{\dagger *} dV} \qquad (6.26)$$

which connects the magnetic field with the magnetization. Q_c and w_c are here the Q and resonant frequency of the cavity in the absence of the magnetization. For stationary states of oscillation, there should be no damping, and $Q_m \rightarrow \infty$. The integrals on the right may be written

$$\frac{\int M^\dagger \cdot H^{\dagger *} dV}{\int H^\dagger \cdot H^{\dagger *} dV} = \frac{1}{H_z} K \overline{M^\dagger}$$

where K is a number depending on the cavity mode distribution. Eqn (6.26) can now be solved for the field H_z in terms of the magnetization M to give

$$H_z = - \frac{4\pi i \overline{M^\dagger} K}{\frac{1}{Q_c}[1+2iQ_c \frac{w-w_c}{w_c}]}$$

Near resonance this can be written

$$H_z = -4\pi i K Q_c \overline{M^\dagger}[1-2iQ_c \frac{w-w_c}{w_c}]$$

Using the amplitudes (6.24), we now compute the magnetization $\overline{M\dagger}$

$$\overline{M\dagger} = \frac{\mu_o I_o x}{aV_{eff}} \int_0^\infty e^{-\gamma t}\left[\frac{i}{2}\sin at + \frac{\lambda}{a}\sin^2 \frac{1}{2}at\right]dt$$

Integrating

$$\overline{M\dagger} = \frac{\mu_o I_o}{V_{eff}}\left[\frac{x}{a} \right]\left[\frac{i}{2} \frac{a}{a^2+\gamma^2} + \frac{\lambda a}{2\gamma(a^2+\gamma^2)} \right]$$

Substituting this result into the expression for H_z, one obtains

$$H_z = 2\pi K Q_c\left[1-2iQ_c \frac{w-w_c}{w_c}\right] \frac{\mu_o I_o}{V_{eff}} \left[\frac{x}{a} \right]\left[\frac{1}{\gamma^2+a^2} \right]\left[1-i\frac{\lambda}{\gamma}\right]$$

The resonance frequency with the magnetization present within the cavity may be found by equating the imaginary part of H_z to zero. One obtains

$$-2Q_c \frac{w-w_c}{w_c} - \frac{\lambda}{\gamma} = 0$$

or

$$w-w_o = -(w-w_c)Q_c\left[\frac{2\gamma}{w_c}\right]$$

or

$$w-w_p = -(w-w_c) \frac{Q_c}{Q_L} \quad .$$

It is seen that the frequency of the hydrogen line is altered or pulled, if w_c is not equal to w_o. Assuming a cavity Q of 1.5×10^4 and a line Q of 1.5×10^9, we see that the cavity must remain tuned to within 10 cps of the hydrogen line in order not to shift the maser signal by more than one part in 10^{13}. If the storage time is longer, the tuning requirements are correspondingly reduced.

Second Order Zeeman Effect

The quadratic field dependence of the hyperfine transition frequency in atomic hydrogen is $2750H^2$ cps, where the static field is given in gauss. The shift in resonance frequency due to a small change in the static field, ΔH, is $5500\ H\Delta H$ cps. If the shift is to be less than one part in 10^{13}, or about 10^{-4} cps, then $H\Delta H$ must be less than 2×10^{-8}. In a static field of one milligauss, for example, any time fluctuation in field must be less than 20 microgauss, or about 2 per cent of the static field. As the static field is reduced, however, the field regulation requirements rapidly diminish.

If there are any static field inhomogeneities over the region of the storage bulb, the motion of the atoms through these static fields gives rise to Fourier components of the field which may lie near the Zeeman frequency corresponding to the $\Delta m_F = \pm 1$ transitions. These transitions reduce the relaxation time within the bulb, and can quench the maser oscillation. If the static inhomogeneities are caused by the Helmholz coils themselves, then reduction of the static field also reduces the inhomogeneities, and hence the amplitude of the Fourier component at any frequency.

Doppler Shift

Atoms which leave the storage bulb through the aperture before they relax have no net translational velocity within the bulb and do not experience a first order Doppler shift. However, if the wall relaxation time is less than the mean geometrical escape time,

the atoms will have a net translational velocity given roughly by the bulb diameter divided by the relaxation time, about 10 cm/sec. If there are running waves in the cavity, this will result in a small first-order Doppler shift. The magnitude of the shift can be estimated from the result of Shimoda et al (SHI 56)

$$w - w_o = \frac{4\pi^2 L}{Q_d \lambda^2} \bar{v}$$

where L is the cavity length, $\bar{v}$ the average translational velocity, and Q_d the Q of the coupling loop. It is assumed that all the power is coupled from one end of the cavity. Inserting the numerical values, $Q_d = 3 \times 10^5$, L = 25 cm, and $\bar{v}$ = 10 cm/sec, we find that $\nu - \nu_o = 10^{-5}$ cps, or one part in 10^{14}. This can be considerably reduced by coupling power out of the cavity symmetrically.

The second order Doppler shift is dependent on the mean squared velocity within the bulb, and is given by

$$\frac{\nu - \nu_o}{\nu} = \left[\frac{v}{c} \right]^2 = 10^{-10}$$

where we have used a mean squared velocity of 9×10^{10} $(cm/sec)^2$ for the hydrogen. The shift is proportional to the absolute temperature, and thus the fractional temperature shift is

$$\frac{\nu - \nu_o}{\nu T} = 3 \times 10^{-13}/^oC$$

so that if the temperature of the bulb is held to 0.3^oC, the maser frequency will not shift by more than one part in 10^{13}.

Anomalous Dispersion Due to Neighboring States

Along with the desired state, the (1,1) state of hydrogen is also focussed into the storage bulb. The presence of the latter state can change the magnetic permeability within the bulb, which in turn changes the resonant frequency of the cavity, providing the rf field has a component perpendicular to the static field. In the usual case, the rf and static fields are made parallel. The change in permeability at the hyperfine frequency ν, due to the presence of the (1,1) state is given by (SHI 56)

$$\Delta\mu = \frac{2\pi n \mu_o^2}{3h(\nu-\nu')}$$

where ν' is the frequency of the (1,1)$\rightarrow$(0,0) transition, and n is the density of atoms in the (1,1) state. In a static field of 0.1 gauss, the resonance term in the denominator corresponds to the (1,0)$\rightarrow$(1,1) Zeeman frequency of about 1.4×10^5 cps. Assuming a flux of the (1,1) state of 10^{12} sec^{-1}, and a storage time of one second, we obtain from the above expression $\Delta\mu = 6 \times 10^{-10}$. From the relation

$$\frac{d\nu}{\nu} = \frac{1}{2}\,\frac{d\mu}{\mu} \quad ,$$

we find $d\nu/\nu = 3 \times 10^{-10}$ as the fractional shift in the resonant frequency of the cavity. From an earlier result, the maser frequency is in turn pulled by an amount

$$\delta\nu_{maser} = \delta\nu_{cavity}\,\frac{Q_c}{Q_L}$$

That is,

$$\delta\nu_{maser} = 10^{-4} \text{ cps.}$$

This does not affect the frequency of the maser oscillation by more than a part in 10^{13}. A static field of 0.1 gauss which is perpendicular to the rf field has been assumed in this calculation, however, and the effect varies inversely proportionally to this field. The effect also vanishes when the rf and static fields are parallel. In both cases, the effect vanishes if an equal density of (1,1) and (1,-1) states are present in the bulb.

Random Noise in the Maser Oscillator

The stability of the maser is limited by two types of random variations: those due to thermal noise fluctuations in the cavity, and those due to fluctuations in the mean number of radiating atoms within the bulb. The latter effect, analagous to shot noise, will subsequently be shown to be $h\nu/kT$ smaller than the effect of the thermal fluctuations and can thus be neglected.

We have previously derived the power spectrum of the maser oscillator as limited by thermal noise within the cavity. This is now related to the observable frequency stability in the absence of systematic shifts, as might be observed in the comparison of two ideal maser oscillators.

Due to the presence of noise in the cavity, there will be an error in the measured phase of the rf field, given by the ratio of the noise amplitude to the signal amplitude. If we denote the phase error by θ, then $\theta = H_n/H_s$, and

$$\theta^2 = \frac{H_n^2}{H_s^2} = \frac{\frac{1}{2}kT}{P_B \cdot \tau_{rad}}$$

since only one mode is excited, and $P_B \cdot \tau_{rad}$ is the average signal energy in the cavity. The phase error is random, but cannot change faster than the correlation time of the oscillator, $t_{corr} = 1/\Delta\nu_L$, where $\Delta\nu_L$ is the width of the hyperfine line. Therefore, after a time t_{obs}, there will be an rms deviation in phase given by

$$\Delta\theta = \sqrt{\frac{t_{obs}}{t_{corr}}}\ \theta = \sqrt{\frac{t_{obs}}{t_{corr}}\ \frac{\frac{1}{2}kT}{P_B \cdot \tau_{rad}}} \quad .$$

The rms deviation in frequency is

$$\Delta f = \frac{\Delta\theta}{t_{obs}} = \sqrt{\frac{1}{t_{obs}\ t_{corr}}\ \frac{\frac{1}{2}kT}{P_B \cdot \tau_{rad}}} \quad .$$

In the usual case, $\tau_{rad} = t_{corr} = 1/\Delta\nu_L$. Substituting $\Delta\nu_L = 1$ cps, $t_{obs} = 1$ second, and $P_B = 5 \times 10^{-12}$ watts, one obtains

$$\frac{\Delta f}{f} = 10^{-14}$$

as the relative stability neglecting systematic frequency shifts.

The effect of variation in the number of radiating atoms in the storage bulb can be treated in a similar manner. In the time interval τ, $I_o\tau$ atoms enter the bulb, with a fluctuation of $\sqrt{I_o\tau}$ in this time. The corresponding power fluctuation in this interval is $\sqrt{I_o\tau}\ \frac{hw}{\tau} = hw\sqrt{I_o/\tau}$, and since $dP/P = dH/2H$, we find

$$\frac{dH}{H} = \frac{1}{2}\sqrt{\frac{1}{I_o\tau}}$$

as the fractional change in the signal amplitude due to random beam

fluctuations. This shot noise also gives rise to random phase variations of this magnitude, such that after time t_{obs}, the rms phase deviation will be given by

$$\Delta\theta = \sqrt{\frac{t_{obs}}{t_{corr}}} \sqrt{\frac{1}{2} \frac{1}{I_o \tau}}$$

or

$$\Delta f = \frac{1}{2} \sqrt{\frac{1}{t_{corr}\, t_{obs}} \frac{hw}{P_B \tau}} \quad .$$

Comparing this quantity with the analagous expression for thermal noise, we see

$$\frac{\Delta f_{shot}}{\Delta f_{thermal}} \approx \frac{hw}{KT}$$

which has the value 2.5×10^{-4} at room temperature. Therefore, shot noise can be neglected in considerations of maser stability.

CHAPTER VIII.

RESULTS

Hydrogen Hyperfine Structure Separation.

Figure 24 of the previous chapter is a block diagram of the microwave receiver used in conjunction with the hyperfine frequency measurements. As discussed in a previous chapter the short term stability of an Atomichron is probably an order of magnitude worse than its long term stability of one part in 10^{10}. Neglecting the frequency standard for the moment, there are still a number of corrections to be made to the counted frequency before an accurate value of the zero-field hyperfine structure separation can be extracted. These corrections are due to the following influences: cavity pulling, correction to the 100 kc/sec counter time base, quadratic magnetic field shift, and wall collision effects.

As shown in Chapter VII, the cavity pulling of the maser frequency can be written

$$\delta\nu_{maser} = \delta\nu_{cavity} \times \frac{Q_{cavity}}{Q_{line}}$$

Since $Q_{line} = 1.5 \times 10^9$ and $Q_{cavity} = 5 \times 10^4$, we have

$$\delta\nu_m = \delta\nu_c \times \frac{1}{30,000} .$$

Measuring the cavity resonance frequency to 300 cps will introduce an error into the measurement of only .01 cps.

The short term stability of the 100 kc/sec counter time base crystal exceeds 2×10^{-8}. As this signal enters into the determination by only a factor of 4, it introduces a negligible error to the precision of this measurement. The absolute frequency of the crystal is counted in terms of the Atomichron by counting the 5 mc/sec standard signal of the latter.

The quadratic field shift is given by the Breit Rabi formula as $2750\overline{H^2}$ cps where $\overline{H^2}$ is the average value over the region of the bulb. As discussed in Chapter VII, the low field Zeeman transitions $(1,0) \rightarrow (1,1)$ and $(1,0) \rightarrow (1,-1)$ can be induced simultaneously with the maser oscillation. These transitions reduce the effective lifetime of the (1,0) state and, depending on the number of atoms undergoing the transition, can either reduce the amplitude of maser oscillation or completely quench the maser. The Zeeman power is radiated through the thin silver coating of the quartz cavity by a coil driven from a HP 606A oscillator. To avoid power broadening, the power level at resonance is reduced to a level only sufficient to halve the normal maser power level. The minimum Zeeman line width observed is about 1.5 kc/sec which can be attributed to field inhomogeneities over the region of the bulb. The Zeeman frequency is related to the field by

$$\frac{\nu_z}{1.4 \times 10^6} = H(\text{gauss})$$

The error in the quadratic field shift is given by

$$\Delta(2750\ H^2) = 5500\ H\ \Delta H \text{ cps} = 5500\ H\ \frac{\Delta\nu_z}{1.4 \times 10^6}\ .$$

Since the static field in the laboratory after compensation is about 80 milligauss, an error in Zeeman frequency of 100 cps introduces an error of only .03 cps. Although the Zeeman transition measures a value of $\bar{H}$, there is negligible error in assuming $H^2 = \overline{H^2}$ in this case.

If a 60 cps magnetic field of the form $H_o \cos 2\pi\nu t$ is superposed on the static magnetic field, the quadratic shift due to this field is

$$\overline{2750\ (H_o \cos 2\pi\nu t)^2} = 1375\ H_o^2$$

An upper limit of $H_o = .005$ gauss was maintained in these experiments as measured by a pick-up coil. This introduces an error of less than .04 cps.

The wall-collision shifts can be treated as in the case of the Cesium experiment in Part I of this paper. As also discussed in Chapter V, the mean phase shift per collision, δ, is related to the frequency shift by

$$\Delta f = \frac{\delta}{2\pi} \cdot \frac{1}{t_o}$$

where t_o is the mean wall collision time. Therefore, measurements of the hyperfine frequency with bulbs of different diameter should determine δ. This assumes that the surface properties, as given by δ, are reproducible from bulb to bulb.

Preliminary Data

The routine followed in measurements of the maser frequency was as follows: The cavity resonance frequency and loaded Q were first measured. This was followed by a Zeeman count, that is, the measurement of the frequency of the low-field Zeeman transitions as detected by reduction of the maser output power. A hyperfine count followed as a series of 10 counts to .1 cps of the 5.7 kc/sec signal. Zeeman counts alternated with hyperfine counts in rapid succession to the extent necessary to obtain reasonable statistics. Runs using the Pierce Hall Atomichron required 6 such sequences although there was no need for such extended counting with the Lyman Laboratory Atomichron used as a standard. The time required to make a complete run never exceeded 30 minutes, and at this time the cavity resonance frequency was remeasured.

At the time of this writing, 29 runs on Dri-Film coated bulbs of two sizes have been made. One bulb was of 6 1/2" diameter with a 4" long 9 mm ID entrance tube, the other bulb was of 4 1/2" diameter with an .080" entrance aperture. The Pierce Hall Atomichron which is operated and monitored by J. R. Pierce was the standard for most of the runs. Tables I and II tabulate the results graphically for the zero field hyperfine structure separation of atomic hydrogen. The minimum error in these determinations is the 0.1 cps counting error of the frequency counter.

The average of 13 runs with the 6 1/2" bulb, with the rms deviation is

$$1420,405,762.17 \text{ cps} \pm 0.4 \text{ cps}$$

and the corresponding numbers for the 4 1/2" bulb are

$$1420,405,762.21 \text{ cps} \pm 0.7 \text{ cps}$$

The deviations among runs on a given bulb are larger than expected, and are due to some systematic error or errors which are as yet not understood. Three possible causes are: the stability of the Atomichron, the fluctuations in the magnetic field, and wall shifts.

The 100 kc/sec signal of the Atomichron was monitored throughout these runs and was found not to vary by more than one part in 10^{10} over any 8 hour period, and by not more than 2 parts in 10^{10} during all the runs. As discussed in chapter VI, the short term stability of the Atomichron is a factor of 10 worse. However, sufficient counts were taken in each run to average out these short term fluctuations. It seems improbable that fluctuations in the Atomichron could normally account for an error in the measurement of more than 0.15 cps.

During the course of several runs, fluctuations in the magnetic field were observed. These fluctuations were always less than 500 cps at the Zeeman frequency, corresponding to a shift in the maser frequency of at most 0.2 cps. Normally, the magnetic fields were essentially constant, and this possible source of error can only be attributed to a few of the experimental runs. The large rms deviation in the measurements with the 6 1/2" bulb cannot reasonable be explained by field drift.

It is not unlikely that wall collision shifts are responsible for some spread in the measurements. Except for the earliest runs, the measurements were made in groups of two, usually separated by a time

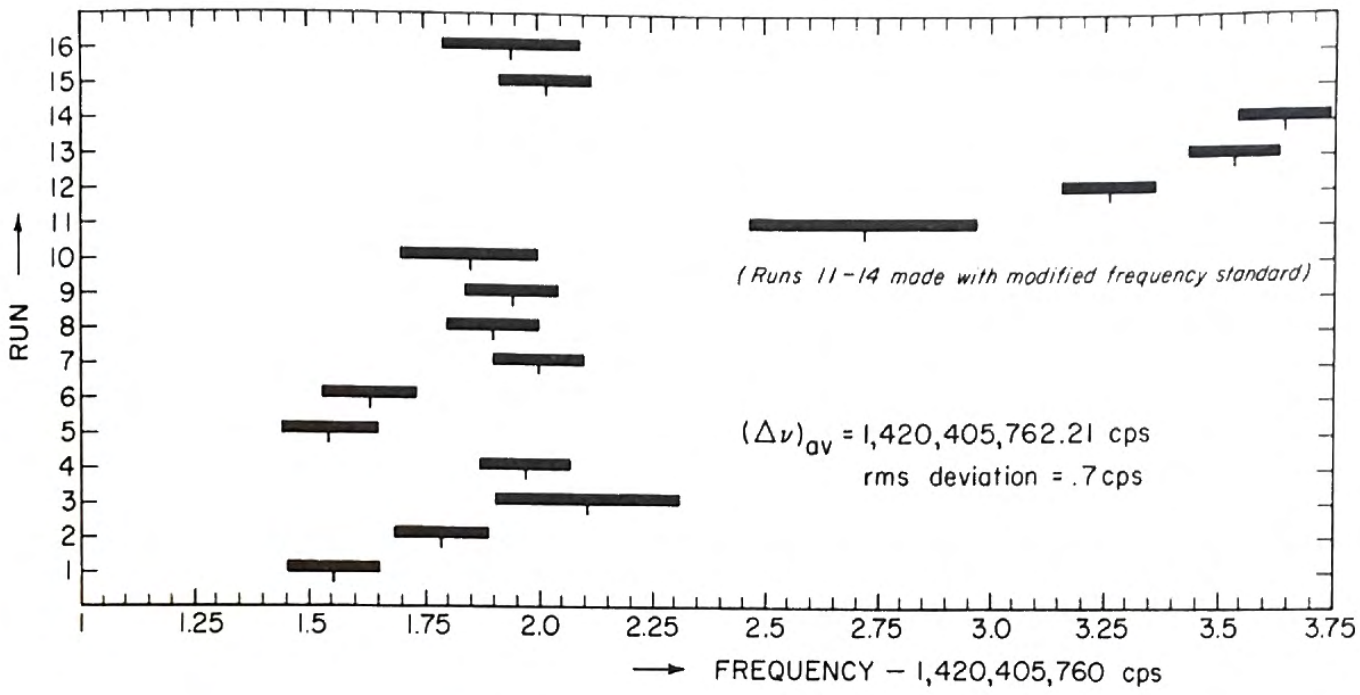

TABLE I. DATA WITH 4½" BULB

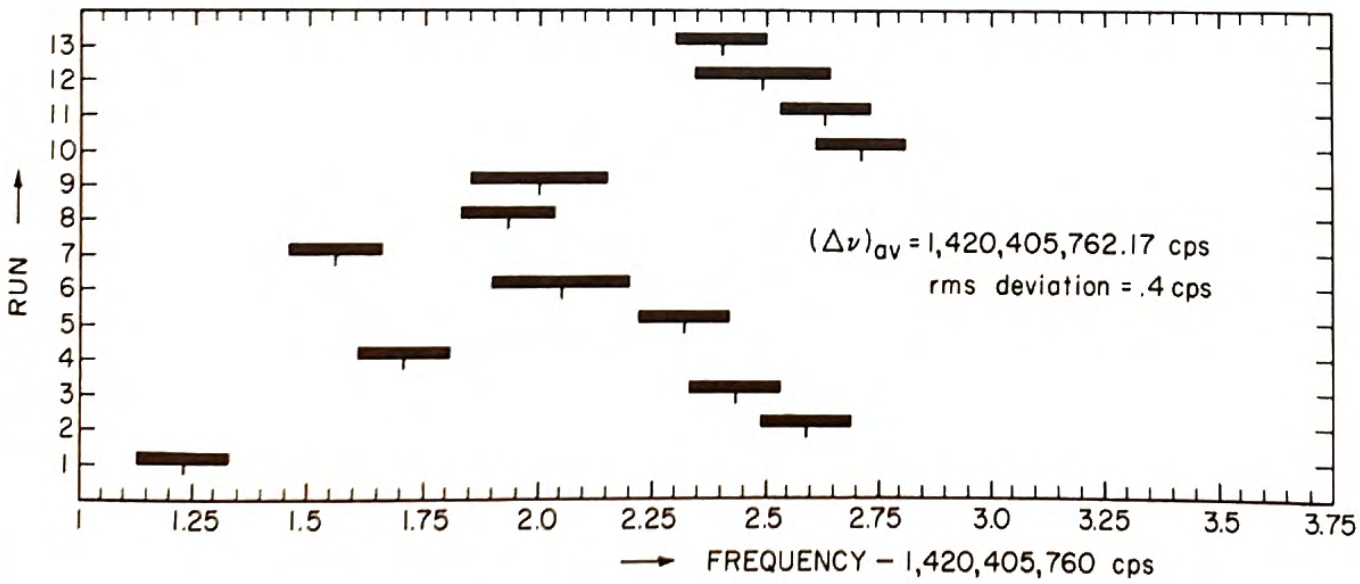

TABLE II. DATA WITH 6½" BULB

of about one hour. It was found that in most but not all instances, good agreement was obtained between successive runs. However, from one 24 hour period to the next, larger shifts were invariably observed.

Interpretation

It is seen that in the data taken with the 4 1/2" bulb, runs 11-14 were shifted an average of 1.5 cps from the rest of the runs. These runs were made with another Atomichron which was discovered to have behaved anomalously during the evening of the data taking. If one deletes these anomalous measurements, the new average for the 4 1/2" bulb runs, with rms deviation is

$$1420,405,761.84 \text{ cps} \quad \pm 0.2 \text{ cps}$$

which is to be compared with the average of the 6 1/2" data:

$$1420,405,762.17 \text{ cps} \quad \pm 0.4 \text{ cps.}$$

It should be noted that the apparent difference in the two frequency determinations is quite comparable to typical deviations among measurements of a given bulb. For a hydrogen velocity of 3×10^5 cm/sec, the frequency shifts can be expressed in terms of the mean phase shift per collision, δ

$$-(\Delta f)_6 = 3 \times 10^4 \delta \text{ cps}$$

and

$$-(\Delta f)_4 = 4.1 \times 10^4 \delta \text{ cps.}$$

where the subscript corresponds to the size of the bulb. If the average difference frequency of the two sets of runs is taken as a wall shift, then $.33 = 1.1 \times 10^4 \delta$, or $\delta = 3 \times 10^{-5}$ rad/coll.

To explain the typical deviation of about 0.3 cps among runs on the 6 1/2" bulb, the mean phase shift per collision, δ would have to vary by an amount Δ, where $3 \times 10^{4}\Delta = .3$, or $\Delta = 10^{-5}$ radians per collision. This is about 30 per cent of the average δ, but this is not unreasonable in view of the sensitivity of δ to the adsorption energy as in (2.24).

An upper limit to the mean phase shift for hydrogen on Dri-Film can be inferred from the data. The frequency difference of the two bulbs is certainly less than 1 cps, and therefore

$$1 > 1.1 \times 10^{4}\delta$$

and thus

$$\delta < 10^{-4} \text{ radians/collision.}$$

The maximum number of bounces which can be used is given by

$$\frac{1}{2} n\delta^2 = 1$$

$$n \approx 2 \times 10^{-8}$$

Assuming there are no other relaxation mechanisms, the storage time obtainable with this number of bounces using a 6 1/2" diameter bulb is about 6000 seconds or 100 minutes.

Pulsed Operation and Relaxation Times

The initial observations of stimulated emission in atomic hydrogen were made using a pulse technique. As discussed in chapter VII, the exponentially decaying power level in the cavity gives a direct measure of the relaxation times of atomic hydrogen in the bulb, assuming the operating conditions are far from oscillation threshold.

Figure 26 is a photograph of a typical oscilloscope trace of the output of the detector phase discriminator. Here the coupling

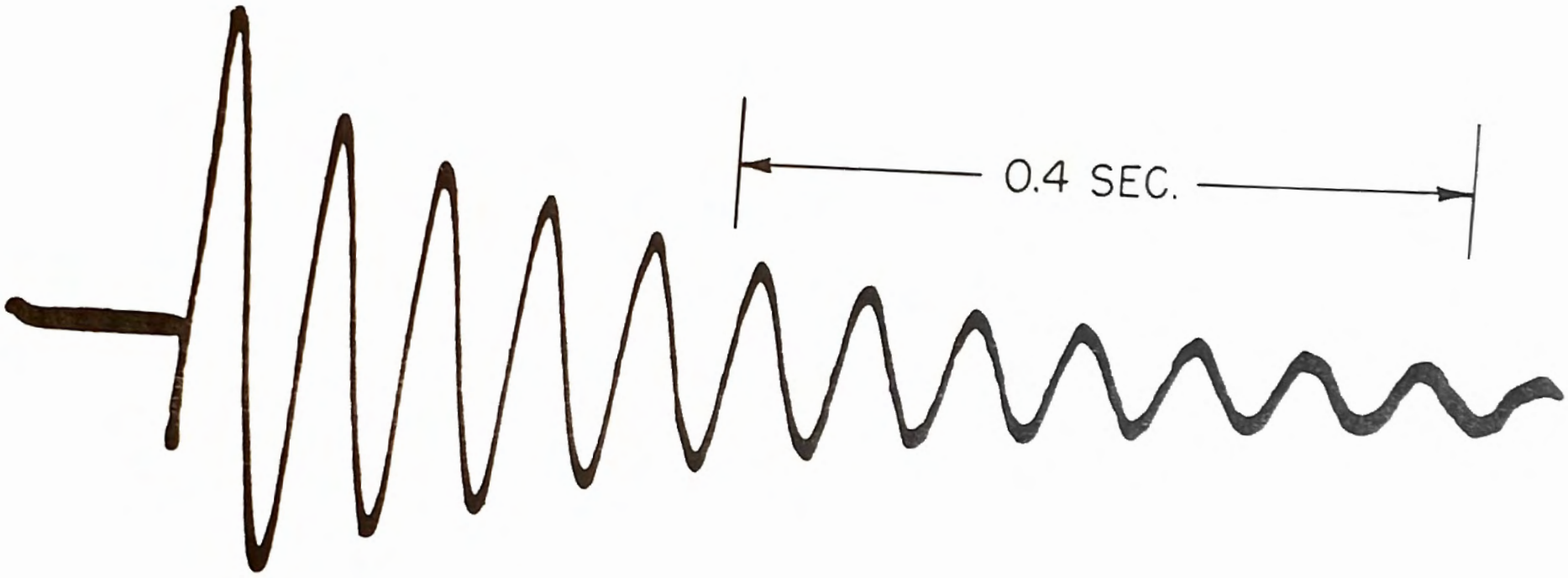

FIG. 26 PULSED STIMULATED EMISSION

loop was adjusted for maximum loading of the cavity. The bulb has a diameter of 6 1/2" with a 4" entrance tube of 9 mm ID. For such a bulb, the relaxation time corresponding to the escape of atoms from the bulb is 200 milliseconds. It is seen from the photograph that the experimental relaxation time is approximately 300 msec. The flux was sufficiently high in this case that even maximum cavity loading could not prevent beam enhancement of the relaxation time. Upon a slight decoupling of the loop, the maser broke into strong oscillation. Using lower fluxes, and another bulb, relaxation times of up to 300 msec have been measured. However, the relaxation times to be expected on geometrical grounds were a full second in these cases.

The first thought is to explain the 0.3 second relaxation time in terms of a wall relaxation effect, but the experimental results on the frequency shifts have set an upper limit to the mean phase shift per collision of 10^{-4} radians. To explain the present relaxation time of .3 seconds, the phase shift per collision would have to be about 0.015 radians, and therefore the wall collisions cannot explain this short relaxation time.

As discussed earlier, it was found that with all transverse components of the magnetic field cancelled out as well as possible, the component along the axis can not be reduced to less than about 50 milligauss without quenching the maser oscillation. This fact can be explained in terms of the transverse inhomogeneities of the Helmholz coils themselves. For small static fields, Fourier components of the inhomogeneous fields at the Zeeman frequency can induce transitions which are similar to Majorana flops within the bulb.

These flops have the same effect on the maser as the externally induced Zeeman transitions used to monitor the magnetic field. That is, the mean lifetime is shortened and the maser oscillation is quenched. It is thought that the measured relaxation time of .3 sec can be explained by this mechanism. It has been found that increasing the z field can increase the relaxation time slightly in some cases, which is consistent with this theory.

Multiple Pulse Methods

In the pulse technique previously described, the pulse repetition frequency is ordinarily so low compared to the relaxation time that there is no phase coherence between atomic states after successive pulses. On the other hand, if the repetition frequency is so high that the time between pulses is less than the relaxation time, states would be expected to be phase correlated for two or more successive pulses. In analogy to atomic beam experiments with separated oscillatory fields, interference effects are to be expected.

The single pulse excitation of the cavity corresponds in the semiclassical description to a flipping of the electron spin by 90° into a radiating state. The response of the spin system to a variable frequency pulse of this type would then have a maximum at the resonance frequency of the transition, with a width equal to that of the Fourier spectrum of the pulse.

If, instead, the pulse length and amplitude are adjusted such that two pulses of rf are required to attain the 90° state, then the system would have a broad response characteristic of the pulse length,

on which is superposed narrower fringes whose width is characteristic of the time between pulses. In the case of high pulsing power, on the other hand, the spectrum of the rf consists of strong sidebands separated by the pulse repetition frequency. As the carrier frequency is swept, the spin system will respond to any sideband satisfying the resonance condition. Therefore, the response of the hydrogen to a high power train of pulses, is a broad response with a large number of subsidiary maxima separated by the repetition frequency.

This characteristic behaviour is illustrated in fig 27. These curves are a measure of the integrated pulsed stimulated emission in the cavity as a function of stimulating frequency.

Direction of Future Work

The techniques developed in this research should make possible a number of interesting experiments. To realize the full capabilities of the technique in high precision rf spectroscopy, it will be necessary to build a second atomic hydrogen maser as comparison standard. With careful design, a stability of one part in 10^{13} should not be an unrealistic figure for both masers. This should allow measurement of the ratios of hyperfine structure separations of the hydrogen isotopes to 13 significant figures. With this stability, the effects of wall collisions can be more accurately measured. This in turn will determine the ultimate limit to the storage time in bulbs of different coatings, and may lead to a better understanding of wall collision interactions.

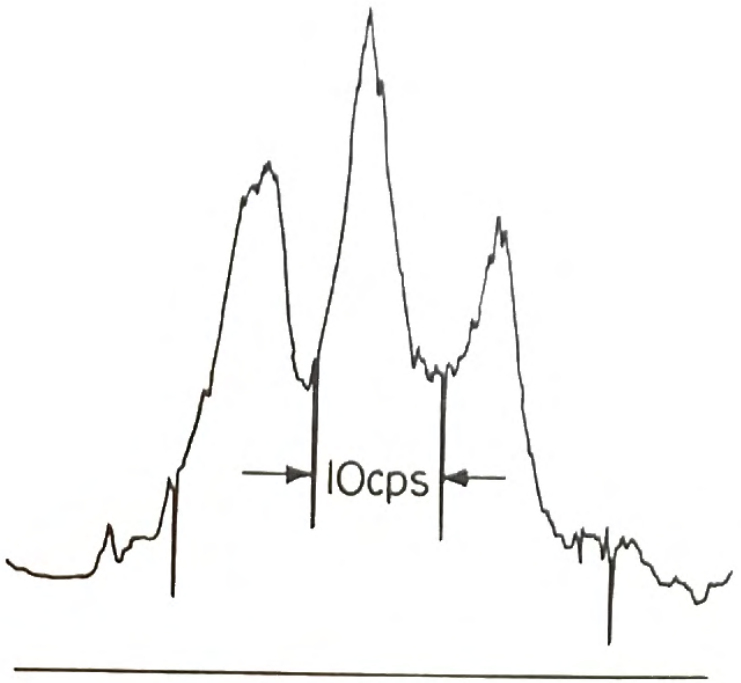

LOW POWER

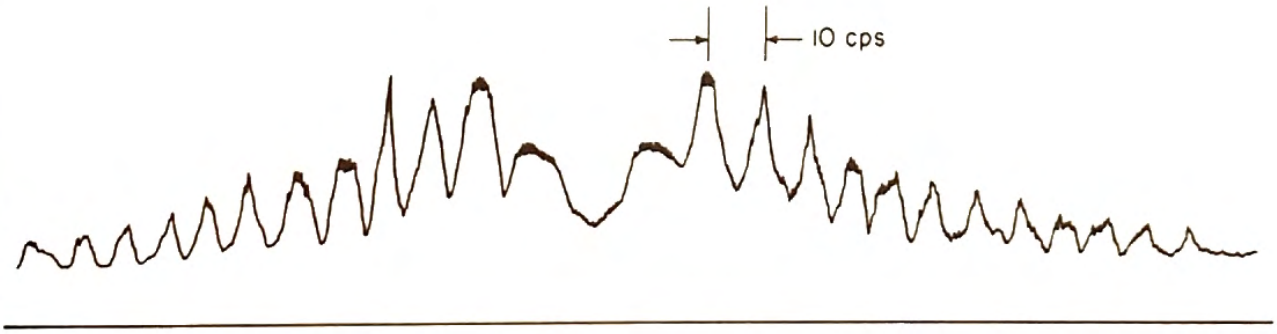

HIGH POWER
PRF = 10 cps

FIG. 27 MULTIPLE - PULSED STIMULATED EMISSION

The g value of the electron is a quantity of considerable theoretical interest. It may be possible to sustain maser oscillation in magnetic fields of sufficient magnitude that the maser frequency just equals the free electron cyclotron resonance frequency in the same field. If free electrons can be obtained in the maser cavity at this magnetic field, it should be possible to measure the magnetic moment of the electron in hydrogen in terms of the free electron moment directly.

The atomic hydrogen density in the storage bulb can be increased to the point that spin-exchange collisions become the dominant relaxation mechanism. Thus it should be possible to obtain a measure of the cross-section for this interaction.

The Breit-Rabi formula has never been checked at extremely low magnetic fields. If the problem of field homogeneities can be adequately overcome, it will be possible to check this formula to high accuracy at extremely low fields.

As a frequency standard the maser should have an extremely high inherent stability, as discussed in chapter VII. It will be necessary to verify these predictions and evaluate the influence of perturbing effects such as stray magnetic fields, temperature variations, and reproducibility of wall collision effects.

The maser can be made quite compact if the source and state selector could be eliminated. An optical pumping scheme might provide the alternative means of obtaining the requisite polarized atomic hydrogen density within the bulb.

Lastly, should the maser indicate a stability which verifies present speculations, it will be possible to perform a number of relativistic clock experiments of unprecedented precision.

APPENDIX A

SOLID ANGLE OF FOCUSSING MAGNET.

In the following calculations, it is assumed that the source lies within the magnet and that the trajectories are sinusoidal. A small correction for the first assumption is made later. The assumption of sinusoidal trajectories is equivalent to that of a fixed magnetic moment for the atom, which is a good approximation for the (1,0) state in hydrogen with the fields used.

$$F_r = m\ddot{r} = -\nabla(-\mu \cdot H) = \mu \frac{\partial H}{\partial r}$$

where

$$H = H_o \, (r/a_o)^2$$

$$r = r_o \sin \frac{2\mu H_o}{ma^2} \, t$$

but

$$x = vt$$

and thus

$$r = r_o \sin \frac{2\mu H_o}{mv^2 a^2} \, x \, .$$

If we chose the most probable velocity in the beam, we obtain

$$r = r_o \sin kx$$

$$k = \sqrt{\frac{2\mu H}{mv^2 a^2}} = \sqrt{\frac{4\mu H_o}{3kTa^2}} \qquad \text{(A.1)}$$

Figure 28 indicates the parameter used in this analysis. Within the magnet, a typical trajectory of the form $r_1 = r_o \sin kx$ is assumed, where r is measured transverse to the beam and x along the axis of the magnet. The origin of coordinates lies at the source. By equating slopes at x = l, the straight-line trajectory outside the magnet is found to be

$$r_2 = r_o [\sin kl + (x-l)k \cos kl].$$

We require the trajectory to intersect the axis at the target:

$$r_2(l+L) = 0 = r_o [\sin kl + Lk \cos kl].$$

Therefore

$$\tan kl = -Lk \qquad (A.2)$$

For focussing trajectories, k is seen to be fixed by the geometry. However, as the target has a radius d, a finite spread of k, Δk, will be focussed, where

$$\frac{\partial}{\partial k} [r_2 (x,k)] \Big|_{\substack{\Delta k = 2d \\ x = L + l}}$$

The derivative of $r(x,k)$ with respect to k

$$r_o [(l + L) \cos kl - Llk \sin kl] = r_o A \qquad (A.3)$$

The parameter A is defined by (A.3) and is a function of the geometry. Therefore we have

$$\Delta k = \frac{2d}{r_o A} \qquad (A.4)$$

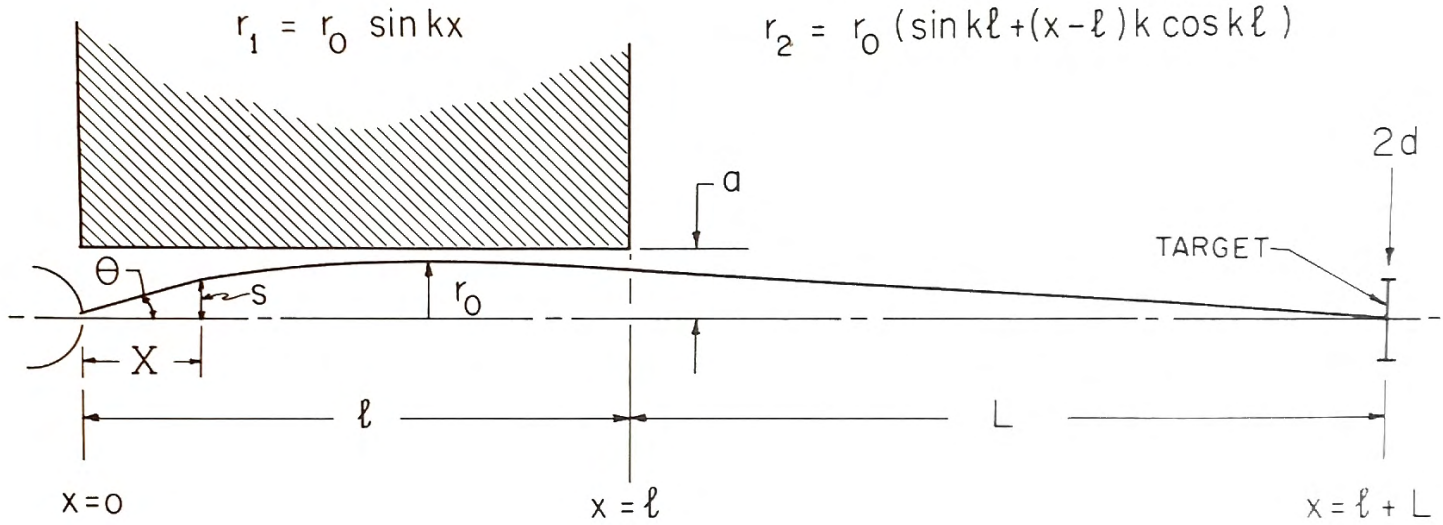
$r_1 = r_0 \sin kx$
$r_2 = r_0 (\sin k\ell + (x-\ell) k \cos k\ell)$
2d
a
TARGET
θ
s
r_0
X
ℓ
L
x=0
x = ℓ
x = ℓ + L

FIGURE 28

That is, the allowed spread in k for any set of trajectories with fixed r_o varies inversely as r_o. Referring to figure 28, the value X is conveniently chosen such that $x < X$.

$$s = r_o \sin kX$$

$$\frac{1}{r_o} = \frac{\sin kX}{s} \tag{A.5}$$

and therefore from (A.4) we have

$$\Delta k = \frac{2d\sin kX}{s} \tag{A.6}$$

which gives the allowed spread in k in terms of a convenient variable s. From (A.1) we see that k varies inversely as the velocity v, and therefore

$$\frac{\Delta k}{k} = \frac{dv}{v} . \tag{A.7}$$

This relates the allowed spread in velocities, dv, to that in k, Δk, as in (A.6). The distribution governing velocities in the beam is a modified Maxwellian distribution (RAM 56).

$$\frac{I(v)dv}{I_o} = \frac{2v^3}{\alpha^4} e^{-(v/\alpha)^2} dv$$

here

$$1/2m^2 = kT$$

r from (A.7)

$$\frac{I(v)dv}{I_o} = \frac{2v^4}{\alpha^4} e^{-(v/\alpha)^2} \frac{\Delta k}{k} .$$

f we let $v = \sqrt{3/2}\alpha$; the most probable velocity in the beam, we have

$$\frac{I(v)dv}{I_o} = \frac{\Delta k}{k} .$$

Therefore, $\Delta k/k$ is the fraction of the beam which will be focussed. We can express the total focussed flux at the target as

$$I_T = \frac{I_o}{\pi} \int_{s_{min}}^{s_{max}} \frac{2\pi s\,ds}{X^2} \frac{\Delta k}{k}$$

or since

$$I_T = \frac{I_o}{\pi} \Omega_{eff},$$

we have

$$\Omega_{eff} = \int \frac{2\pi s\,ds}{X^2} \frac{2d}{Ak} \frac{\sin kX}{s} ,$$

$$= \frac{4\pi d \sin kX}{kAX^2} \int_0^{a\sin kX} ds$$

or

$$\Omega_{eff} = \frac{4\pi a d \sin^2 kX}{kAX^2} . \qquad (A.8)$$

The result expresses the effective solid angle for a source within the magnet. If the source lies a distance R_s outside the magnet entrance, the expression is corrected by the factor $(X/R_s)^2$, where the optimum value of R_s is given by

$$r_o \sin kX = R_s r_o k \cos kX \qquad (A.9)$$

and

$$\Omega_{eff} = \frac{4\pi a d \sin^2 kX}{kAR_s^2} . \qquad (A.10)$$

As a numerical example, let l = 12", L = 48", 2d = 0.080", X = 4", and a = .23". Then, from (A.2) we find k = .132 inch^{-1} and therefore sin kX = .505. Applying (A.3) we find A = 75.1, while from (A.9) we

obtain R_s = 4.45". Substituting these values into (A.10), we finally obtain $\Omega_{eff} = 1.5 \times 10^{-4}$ steradians.

The requisite magnetic field strength may be calculated from (A.1) using the calculated value of k = .132 to obtain

$$H(\text{gauss}) = \frac{3kTa^2}{4\mu} k^2$$

= 3000 gauss at room temperature.

In the present magnet, we have not been able to maximize the focussed flux for fields of up to approximately 5500 gauss. This would suggest that the most probable velocity in the beam is characteristic of a temperature appreciably higher than room temperature.

APPENDIX B

CAVITY FIELD AVERAGES

The magnetic fields within a cylindrical cavity resonant in the TE_{011} mode are given by (MON 48)

$$H_z = H_o J_o(kr)\sin\frac{\pi z}{L}$$

$$H_r = \frac{\pi}{kL} H_o J_o'(kr)\cos\frac{\pi z}{L}$$

$$H_\theta = 0$$

where $J_o'(ka) = J_1(ka) = 0$, or $ka = 3.832$. The resonant wavelength is related to the cavity dimensions through

$$(1/\lambda)^2 = (1/2L)^2 + (k/2\pi)^2$$

where L and a are the cavity length and radius respectively. If we assume a cavity with $2a = L$, we obtain for a resonant frequency of 1420 mc/sec the value $L = 27.78$ cm.

The two quantities of greatest interest are the mean squared value of the total magnetic field over the entire cavity, and the mean value of the z component of the field over the region of the storage bulb. It is not clear how the quartz bulb affects the mode distributions, and these calculations assume that the field distributions remain unchanged by the bulb. The mean squared value of the field is given by

$$\overline{H^2} = \frac{1}{V}\int \frac{H^2}{2}\, dV = \frac{\pi}{V}\int\int \left(H_r^2 + H_z^2 \right) r\,dr\,dz$$

$$\overline{H^2} = \frac{\pi H_o^2}{V}\left[\int_0^a\int_0^L J_o^2(kr)\sin^2\frac{\pi z}{L}\, r\, drdz + (\pi/kL)^2\int_0^a\int_0^L J_1^2\cos^2\frac{\pi z}{L} rdrdz\right]$$

$$\overline{H^2} = \frac{\pi H_o^2 L}{V}\left[\int_0^a J_o^2(kr)rdr + (\pi/kL)^2\int_0^a J_1^2(kr)rdr\right]$$

The integrals over r are given by (MAC 34)

$$\int_0^a rJ_o^2(kr)dr = \frac{r^2}{2}\left[J_1^2(kr) + J_o^2(kr)\right]\Big|_0^a = \frac{a^2}{2}J_o^2(ka),$$

$$\int_0^a rJ_1^2(kr)dr = \frac{r^2}{2}\left[J_1'^2(kr) + \left(1-\frac{1}{k^2r^2}\right)J_1^2(kr)\right]\Big|_0^a .$$

Now, we have $J_o'(x) = J_1(x)$, and $J_1(ka) = 0$. Therefore

$$\int_0^a rJ_1^2(kr)dr = \frac{a^2}{2}J_1'^2(ka),$$

and since $J_1'(z) = \frac{1}{z}J_1(z) - J_2(z)$,

we obtain

$$\int_0^a rJ_1^2(kr)dr = \frac{a^2}{2}J_2^2(ka).$$

Lastly, since $J_o(x) = -J_2(x)$, we obtain the result

$$\overline{H^2} = \frac{\pi H_o^2 L a^2}{4\pi a^2 L}J_o^2(ka)\left[1 + (\pi/kL)^2\right]$$

$$\overline{H^2} = H_o^2\frac{J_o^2(ka)}{4}\left[1 + \frac{1}{4}(\pi/kL)^2\right]$$

or since $J_o(ka) = -0.4028$, one obtains $\overline{H^2} = 0.0474\, H_o^2$

The phase of H_z reverses in the TE_{011} mode beyond a certain radius which is given by the first zero of $J_o(z)$. If r_c denotes this radius, then $J_o(kr_c) = 0$ implies $kr_c = 2.405$. We also note that $J_1(2.405) = -0,5191$. The space average of H_z over the storage bulb dimensions is approximated by the following integral

$$\overline{H_z} = \frac{2\pi}{V_{eff}} \int_{L/4}^{3L/4} \int_{0}^{r_c} r\, H_z dr dz$$

$$\overline{H_z} = \frac{2\pi H_O}{V_{eff}} \int_{0}^{r_c} r J_o(kr) dr \int \sin\frac{\pi z}{L}\, dz$$

$$\overline{H_z} = \frac{2\pi H_o L\ 2}{\pi V_{eff}} \int_{0}^{r_c} r J_o(kr) dr$$

The integral is given by

$$\int_{0}^{r_c} r J_o(kr) dr = \frac{1}{k^2} \int_{0}^{kr_c} x J_o(x) dx$$

$$= \frac{1}{k^2}\, x J_1(x) \Big|_{0}^{kr_c}$$

Therefore, one obtains

$$\overline{H_z} = \frac{2\pi H_o 2L\ 2\ r_c}{\pi r_c^2 L \pi k}\, J_o'(kr_c)$$

$$\overline{H_z} = 0.30\ H_o$$

Using this and the previous result, we find $\overline{H_z} = (.30)(1/.0474)^{\frac{1}{2}} (\overline{H^2})^{\frac{1}{2}}$,

or

$$\overline{H_z} = 1.37 \ [\overline{H^2}]^{\frac{1}{2}} \quad .$$

We may now compute the total average stored energy within the cavity, which is given by

$$\overline{W} = \frac{1}{8\pi} \int \frac{1}{2}(H^2 + E^2)dV \quad ,$$

$$\overline{W} = \frac{1}{4\pi} \int \frac{H^2}{2} \, dV \quad .$$

The integral has been calculated. Thus

$$\overline{W} = \frac{1}{4\pi} \overline{H^2} V = \frac{.0474}{4\pi} H_o^2 V \, .$$

The result can also be written

$$\overline{W} = \frac{V}{4\pi} \quad \frac{.0474}{.09} \quad (\overline{H_z})^2$$

$$\overline{W} = \frac{.528}{4\pi} [\overline{H_z}]^2 V$$

REFERENCES

ADR 60 F. J. Adrian, Jour, Chem. Phys. 32, 972 (1960).

AND 60 L. W. Anderson, F. M. Pipkin, J. C. Baird, Phys. Rev. Letters 4, 69, (1960) .

BEN 58 P. L. Bender, E. C. Beatty, Phys. Rev. 112, 450(1960).

BLO 56 S. Bloom, Jour. App. Phys. 27, 785 (1956) .

BOE 50 J. H. de Boer, Advances in Colloid Science, Interscience Publishers (1950).

BOE 53 J. H. de Boer, Dynamical Character of Adsorption Clarendon Press (1953).

ESS 59 Proceedings 13th Annual Symposium on Frequency Control May (1959).

DIC 54 R. H. Dicke, Phys. Rev. 93, 99 (1954).

DIC 55 R. H. Dicke, R. H. Romer, Rev. Sci. Inst. 26, 915 (1955).

FRA 59 W. Franzen, Phys. Rev. 115, 850 (1959).

FRI 51 H. Friedburg, W. Paul, Naturwissenschaften 38, 159 (1951).

FRI 59 This sample was kindly supplied us by Prof. Friedburg .

GEN 60 General Electric Silicone Prod. Div. Waterford NY,SC-02.

GOR 55 J. P. Gordon, H. J. Zeiger, C. H. Townes, Phys. Rev.99, 1264 1955

HIR 54 J. Hirschfelder, C. F. Curtiss, R. Bird, Molecular Theory of Gases and Liquids John Wiley and Sons (1954).

JEN 60 S. N. Foner, E. L. Cochran, V. A. Bowers, C. K. Jen, Jour. Chem. Phys. 32 963 (1960).

KLE 58 D. Kleppner, N. F. Ramsey, P. Fjelstad, Phys. Rev. Letters 1, 232 (1958).

KLE 59 D. Kleppner, Thesis, Harvard University, 1958.

KAS 50 A. Kastler, J. Phys. et Rad. II, 255 (1950).

KNA 29 F. Knauer, O. Stern, Zeit. f. Phys. 53, 766 (1929).

MAC 34 N. W. McLachlan,Bessel Functions for Engineers Oxford University Press, (1934).

MAR 39 H. Margenau, Rev. Mod. Phys. 11, 1 (1939)

REFERENCES (contd)

MAR 59 H. Margenau, P. Fontana, L. Klein, Phys. Rev. 115 87 (1959).

MON 48 C. G. Montgomery, Techniques of Microwave Measurements McGraw Hill Book Company 1947.

PAR 59 Paraflint supplied by Moore and Munger, New York, NY.

QUI 56 W. Quinn, Thesis, Harvard University, 1956.

RAM 56 N. F. Ramsey, Rev. Sci. Inst. 28 58 (1956).

RAM 56a N. F. Ramsey, Molecular Beams, Oxford University Press, 1956.

SAG 60 Model 2523, Sage Laboratories Inc. Natick Mass.

SHI 56 K. Shimoda, T. C. Wang, C. H. Townes, Phys. Rev. 102 1308 (1956).

SLA 46 J. C. Slater, Rev. Mod. Phys. 18, 441 (1946).

SYN 60 Supplied by Synchor Products Inc. Malden Mass.

WIT 56 J. P. Wittke, R. H. Dicke, Phys. Rev. 103, 620 (1956)

ACKNOWLEDGMENTS

It is a pleasure to express my sincere appreciation to Professor Norman F. Ramsey for his guidance, his encouragement, and his enthusiasm durning the course of this research.

The work was done in close collaboration with Dr. Daniel Kleppner. His patience, perseverance, and experience have made these years of partnership both pleasant and productive.

To Paul Fjelstad, my admiration and appreciation for many informative discussions, and to Norval Fortson, my gratitude for his considerably assistance on the experiment.

I am indebted to the International Business Machine Corporation for a fellowship in 1957, and to the National Science Foundation for support in 1959 and 1960.